

# Tidal Coulomb Failure Stresses in the Northern Andean intermediate depth seismic clusters and its implications for a possible correlation between tides and seismicity

*Gloria A. Moncayo<sup>a</sup>, Gaspar Monsalve<sup>b</sup> and Jorge I. Zuluaga<sup>a</sup>*

<sup>a</sup> Solar, Earth and Planetary Physics Group, Computational Physics and Astrophysics Group, Instituto de Física-FCEN, Universidad de Antioquia, Calle 70 No. 52-21, Medellin, Colombia

<sup>b</sup> Departamento de Geociencias y Medioambiente, Facultad de Minas, Universidad Nacional de Colombia, Carrera 80 No. 65-223, Núcleo Robledo, Medellín, Colombia

## Abstract

A recent statistical analysis of the relationship between tides and seismic activity in Colombia has suggested the existence of correlation anomalies for the case intermediate depth events in the Bucaramanga nest and the Cauca cluster (Moncayo et al., 2018). In this work, we explore in detail the hypothesis that tides may be triggering seismic activity in these regions and extend the analysis to two other seismic clusters in the northern part of South America, specifically in the areas of Puyo (Ecuador) and Pucallpa (Peru). For this purpose, we use the available focal mechanism information for almost hundred events in the area, and calculate for each event the Tidal Coulomb Failure Stress (TCFS) as obtained from estimations of the tidal strain tensor. Tidal strains are computed considering both, the Earth Body Tides (BT) and the effect of the Ocean Tidal Loading (OTL). Since our purpose is to elucidate the role of tides in earthquake nucleation, calculations of the TCFS are made not only for the time of earthquake, but also for the time of the closest maximum strain within a window of a few hours before the events. Our results tend to support the hypothesis that tidal stresses are contributing to earthquake generation in all the studied areas. Additional tests on the earthquakes within the Bucaramanga nest indicate that the monthly phase is the main tidal contributor to the earthquake generation process. Our results are in agreement with the suggestion that in the zones of seismic clusters, and given their intermediate depth conditions where compressional stresses are expected (Turcotte and Schubert, 2002), the lunisolar forces may contribute to facilitate the displacement of blocks, and hence the triggering of seismic activity.

**Key words:** Tidal Coulomb Failure Stress, Bucaramanga seismic nest, Cauca seismic cluster, Puyo seismic swarm, Pucallpa seismic swarm, seismic clusters, tidal triggering.

## 1. Introduction

An earthquake occurs when a sudden release of mechanical energy takes place within the crust, at the hypocenter, where deformations have accumulated over years, decades or centuries. The generation of an earthquake can be described with the so-called seismic cycle (Fedotov, 1965). During one of the phases of this cycle (the interseismic phase), the accumulation of strain brings the system to a critical state that ultimately leads to the occurrence of the earthquake (coseismic phase). Although the origin of the stresses involved in the seismic cycle is mostly endogen (tectonic, volcanic, etc.), we could ask whether, in addition to the endogenous contribution, there could be other phenomena involved in triggering the seismic event. One of these phenomena is the tidal stresses, built upon the gravitational interaction of the Earth with the Sun and the Moon. Despite being two or three orders of magnitude smaller than the typical stress drops, tidal strains induce stress rates even greater than the tectonic ones (Emter, 1997).

For more than a hundred years, the idea of a relationship between tides and seismicity in the Earth has attracted the attention of scientists around the world. Many works in the area have been published in the last two decades, focusing on both global and regional seismic contexts (see eg. Emter, 1997; Tanaka et al., 2002; Métivier et al., 2009; Wilcock, 2009; Tiwari et al., 2014; Moncayo et al., 2018). Most of these studies have focused on the direct effects of tides on tidal triggering, namely the effect of solid or body tides as measured at or around the hypocenter of the earthquake. Others, however, have also included the so-called indirect effects of the tides (see e.g. Tsuruoka et al., 1995; Vidale et al., 1998; Cochran et al. 2004; Tanaka et al., 2002, 2004, 2006, Tanaka 2010, 2012; Arabelos et al., 2016), namely, the effect that ocean tides could have in tidal triggering.

The indirect effect is important because in continental areas close to oceanic basins, the Ocean Tidal Loading (OTL) could produce stress changes with amplitudes comparable to those of the solid earth tides (Tsuruoka et al., 1995). More interesting is the fact that OTL may disturb the faults by a hold-and-release mechanism, arising from variations in water mass over the ocean basin (Cochran, 2004). This effect may produce a slightly different effect than those expected by studying only the body tides.

Since the OTL effect near ocean margins can be larger than the solid earth tides (e.g. Tanaka et al., 2002), its role as a triggering mechanism should not be overlooked. Modeling the OTL is more difficult than modeling solid Earth tides (Agnew, 2007). This fact has delayed the reliable study of these effects on tidal triggering with respect to what have been done with body tides. However, recent technological tools and improved geographical models of the ocean basins worldwide, have contributed to improve the estimation of the effect.

In a previous work, we reported the discovery of correlation anomalies (anomalously low p-values of the Schuster Statistical Test) between intermediate depth seismicity in the Bucaramanga nest and Cauca cluster in Colombia (Moncayo et al., 2018) and the diurnal and monthly phase of the body tides. In that study, we neglected the

indirect effect of OTL arguing that typical distances of the seismic clusters to the Caribbean and Pacific coasts were relatively large (200-500 km). Since the OTL decreases with distance to the coasts (e.g. Matsumoto et al., 2001; Wendt, 2004), we assumed that considering its effects on the statistical results we found in that study, was not mandatory.

In this work, we revisit the problem and study tidal triggering in the aforementioned seismic clusters, including now the indirect effect of the OTL. Moreover, we go a step further by including in our analysis other two high seismicity areas close to the West Coast of South America, namely the Puyo (Ecuador) and Pucallpa (Peru) seismic swarms, where a noticeable concentration of intermediate-depth events have been observed (Zarifi and Havskov, 2003; Soles Valdivia, 2012; Taibe, 2013). In Moncayo et al. (2018) we focused on devising novel approaches to compute the tidal phases and to perform the statistical analysis of their correlation with seismicity. In that study, we applied our methods to samples of earthquakes with a statistically significant number of events. In this paper, we focus on much smaller samples, namely, those formed by earthquakes whose focal mechanisms are reliably determined. For each earthquake we compute the local value of the tidal strain, and from them we estimate the so-called Tidal Coulomb Failure Stress (TCFS).

Other authors have attempted to study the TCFS in relation with tidal triggering (e.g. Smith and Samis, 2002; Cochran et al., 2004; Fischer et al., 2006; Xu et al., 2011; Gallego et al., 2013; Miguelsanz del Álamo, 2016; Bucholc and Steacy, 2016). Thus, for instance, Smith and Samis (2002) include the tidal Coulomb effective stress response in their analysis of the Northridge and Loma Prieta earthquakes. Independently, Cochran et al. (2004) performed an analysis of worldwide earthquakes considering shear and normal stresses, and found a significant tidal correlation for large tectonic events with increasing tidal stress amplitudes. Fischer et al. (2006) studied the possibility of tidal triggering for an earthquake swarm in the NW-Bohemia/Vogtland region, in Central Europe. In their study they considered only solid Earth tides, due to the large distances between the studied region and the Mediterranean Coast; they reported no significant tidal correlation with the swarms in the region. Xu et al. (2011) conducted a global study of the TCFS with shallow (<60km) and large ( $M > 5$ ) earthquakes for different types of faults. They found a dependence of the TCFS with latitude. In the case of thrust faults, they found increased cases of tidal slip, especially for middle and high latitudes. On the other hand, normal faults seem to be more propense to tidal slip at low latitudes, while in the case of strike-slip faults the effects are reduced with latitude. These authors suggested that the properties of the TCFS are closely related to the fault type, location and strike. More recently, Gallego et al. (2013) analyzed the possible contribution of the solid Earth tides and the OTL in the tremor occurrence around the Chile triple junction region. They found a maximum correlation for Coulomb stresses for faults subparallel to the subducted transform faults. Moreover, they found that the combined effect of both, solid earth tides and OTL may facilitate or prevent tremor production in the area. The most recent cases of TCFS analysis are those of Miguelsanz del Álamo (2016) and Bucholc and Steacy (2016), both focusing in the very well-known California seismic area. The former, proposed new methods to

solve the problem of the true nodal plane determination in the focal mechanisms (which is a key problem when analyzing the correlation between the TCFS and tides) and found significant correlations between the maximum TCFS and the time of occurrence of earthquakes. Bucholc and Steacy (2016), on the other hand, analyzed both solid Earth tides and OTL and found a correlation between tidal triggering and the magnitude of the tidal stresses.

Earthquake tidal triggering for intermediate-depth earthquakes and/or in seismic nests is not a new research topic (e.g. Curchin and Pennington, 1987; Cadicheanu et al., 2007; 2014). Curchin and Pennington (1987) studied intermediate-depth earthquakes worldwide using only earth tides; they did not find a significant tidal correlation for most intermediate-depth earthquakes. Cadicheanu et al., (2007) considered the fact that the lunisolar attraction can modulate the intermediate depth seismicity and found for the Vrancea zone a significant tidal triggering correlation. In Cadicheanu et al., (2014), the authors searched for some kind of tidal triggering in the three most known seismic nests on Earth: Vrancea (Romania), Bucaramanga (Colombia) and Hindu Kusch (Afghanistan), using a 3D statistical tidal tomography. They found only for Vrancea zone a favorability of tidal triggering, but not for Bucaramanga nor Hindu Kusch. In Bucaramanga they suggested that the time periods between the earthquakes are not associated to tidal triggering (Cadicheanu et al., 2014). They do not use the TCFS in their study. Moreover, and as we argued in our recent work (Moncayo et al., 2018), tidal phases have been improperly computed, especially in the case of the diurnal and monthly phases, in such a way that in most cases, including probably that of Cadicheanu et al. (2014), the strong diurnal and monthly correlations we have observed, have been mostly absent.

This paper is organized as follows: in **Section 2** we start by describing the tectonic setting of the analyzed areas. In **Section 3** we briefly summarize our methods to calculate the direct and indirect effects of tides on Earth for the purpose of our work. **Section 4** describes in detail the calculation of the tidal Coulomb failure stress and the main assumptions behind it. In **Section 5** we present the methods we applied to compute and analyze the TCFS in the studied seismic clusters. **Section 6** presents the results of our computations and a discussion of their implications. Finally, in **Section 7** we summarize our work and draw the most important conclusions derived from it.

## **2. Tectonic setting around the seismic clusters**

The West Coast of South America is characterized by the presence of the Andes mountain range. The Andes Cordillera is the highest non-collisional range worldwide (Ramos, 1999). Several authors distinguish between three different segments in the Andes (see e.g. Gansser, 1973; Ramos, 1999), according to their geological processes and tectonic settings: Northern, Central and Southern Andes. The Northern Block of the Andes (approximately between 12° N and 4°S) is an interaction zone of three tectonic plates: South America, Nazca and Caribbean; and comprises mostly the territory of Colombia, northern Ecuador, and northwestern Venezuela.

The Central Andes (4°- 46°30' S), correspond to the typical Andean-type orogeny associated to the subduction process (Ramos, 1999), with a flat-slab segment observed in the Peruvian Andes (Ramos, 1999). The Southern Andes (46°30'-52° S) correspond to the southernmost part of the range. They are located south of the triple junction between the Nazca, South America and Antarctic plates (Ramos and Kay, 1992).

In the northern Andean Block and the Central Andes, the region containing the 4 seismic clusters we are interested in (Figure 1), the coast is influenced by the subduction of the Nazca plate under the South American plate, at a relative velocity of about 5.3 cm/yr (Sella et al., 2002). The subduction of the Nazca Plate in this area seems to be segmented, with a boundary at ~5° N, where flat subduction occurs to the north and a steeper subduction takes place to the south (Vargas and Mann, 2013; Chiarabba et al., 2015; Syracuse et al., 2016). In northern Colombia, the Caribbean plate seems to subduct at a shallow angle at an average rate of 1 - 2 cm/yr. (Taboada et al., 1998; Trenkamp et al., 2002). The convergence of these plates, plus the presence of at least two microplates or blocks (Panamá-Chocó and North Andes Blocks), and the existence of several active faults, make the region seismically active and tectonically complex (e.g. Pennington, 1981; Pulido et al., 2003; Cardona et al., 2005).

The flat slab subduction zone in Peru is located between 3° and 15° and extends over a length of 1500 km, showing the typical absence of volcanism (see e.g. Barazangi and Isaaks, 1976; Gutscher et al., 2000; Tavera and Buforn, 2001; Eakin et al., 2014). Another characteristic of this zone is the presence of the Nazca Ridge between 14° and 17°, whose subduction can influence the deformation of the mantle in the area (Eakin et al., 2014).

In this tectonic context, we may identify 4 regions where an anomalous concentration of intermediate-depth earthquakes takes place (events marked with stars in Figure 1): 1) the Bucaramanga seismic nest (lat. +7°N, long. 73°W), 2) the Cauca seismic cluster (lat. 4.5°N, long. 76°W), 3) the Puyo seismic cluster (lat. 2°S, long. 78W), and 4) the Pucallpa seismic cluster (lat. 8° S, long. 74° W,).

The Bucaramanga seismic nest corresponds to a concentration of intermediate-depth earthquakes with a mean hypocentral depth of 160 km, which shows the highest concentration of intermediate-depth seismicity worldwide (Prieto et al., 2012). Several authors have tried to explain the origin of this seismic nest (Zarifi and Havskov, 2003; Zarifi et al., 2007; Prieto et al., 2012 and Chiarabba et al., 2015). It is still unclear if the Bucaramanga seismic nest is associated with the Nazca Plate (Chiarabba et al., 2015, Syracuse et al., 2016, Gutscher et al., 2000) or the Caribbean Plate (Van der Hilst and Mann, 1994, Sanchez Rojas and Palma, 2014, Yarce et al., 2014, Idarraga-García et al., 2016). The Cauca seismic cluster is likely related to the subduction of Nazca beneath the North Andean Block (Cortes and Angelier, 2005; Chang et al., 2017). Both the Bucaramanga and Cauca seismic clusters show homogenous stress regimes, with conspicuous E-plunging extensional axis, as mentioned by Cortes and Angelier (2005). An in-depth analysis of the potential correlation between seismicity and earth tides in those clusters was

carried out recently by Moncayo et al. (2018), finding anomalously low values of the Schuster test p-values for the diurnal and monthly tidal components. Those findings motivated this follow-up investigation.

The seismic swarm of Puyo is characterized by events with depths between 130 and 220 km. Most of them have normal mechanisms (Taibe, 2013), which make them very interesting for an analysis of tidal correlation. Zarifi and Havskov (2003) suggested a possible volcanic origin for this cluster, but its nature is still very uncertain. The Pucallpa cluster, on the other hand, is described in the literature as a seismic swarm with an extensive regime (Soles Valdivia, 2012). This concentration of events is located at a distance of 600 to 700 km from the trench, and most of the events have depths between 100 and 190 km (Soles Valdivia, 2012). Evidence has shown since 1970 that seismic activity in the Pucallpa area is larger than in the surroundings, which agrees with the expected characteristics of a seismic nest instead of a swarm (Zarifi and Havskov, 2003; Prieto et al., 2012). Seismic events in the Pucallpa region, show a tendency to be originated in a region parallel to the Cordillera, with a slight deflection to the west (Soles Valdivia, 2012). As suggested by Moncayo et al. (2018) this meridional orientation may favor the effect of tidal stresses. If this is the case, the Pucallpa seismic cluster could be associated with a possible resubduction process (Schneider and Sacks, 1988; Tavera and Buforn, 2001; Soles Valdivia, 2012).

### 3. Calculation of tides and Ocean Tidal Loading (OTL)

Between the two direct effects caused by the gravitational attraction of the Moon and Sun, solid Earth and ocean tides, the former can be described more easily (e.g. Farrell, 1972, 1973; Scherneck, 2001; Zahran et al., 2005; Agnew, 2007). The Ocean Tide Loading (OTL) calculations require the computation of the Love numbers of the liquid ocean (Farrell, 1972). In order to obtain the OTL, it is necessary to consider a model of the ocean tides and the elastic properties of the Earth (e.g. Zahran et al., 2005; Doan et al., 2006; Agnew, 2007). The effect of ocean loading in a given place is computed by the convolution of ocean tidal data with Green's functions (e.g. Farrell, 1972; 1973; Baker, 1984; Jentzsch, 1997; Tanaka et al., 2002; Tanaka, 2010, 2012; Doan et al., 2006; Penna et al., 2008). The OTL displacement  $u(\vec{r})$  at a given point can be written in the following form (Farrell, 1973):

$$u(\vec{r}) = \int_{\Omega} \rho G(|\vec{r} - \vec{r}'|) H(\vec{r}') d\Omega \quad [1]$$

where  $\rho$  is the density of sea water,  $G$  represents the Green's function, which depends on the distance between the position vectors on the Earth's surface  $\vec{r}$  and  $\vec{r}'$  (Farrell, 1973), and  $H$  corresponds to the tidal amplitude at  $\vec{r}'$ . The integral is calculated over the total area of water described by  $\Omega$ .

Considering that the response of the ocean to the tidal forces is not uniform, both phenomena, solid Earth tides and OTL, are generally not in phase (Jentzsch, 1997;

Wilcock, 2009). Another aspect to consider is that the local properties of the crust and mantle affect the OTL, whereas the solid or body tides depend on the global properties of the Earth (Farrell, 1972).

The OTL effect decreases with distance to the seashore (e.g. Doan et al., 2006). Several studies highlight the role that the OTL plays in the search for a correlation between tides and seismicity, which is a factor that cannot be neglected, especially if the seismic events are located in areas near the coasts (e.g. Tsuruoka et al., 1995; Jentzsch et al., 2001; Wilcock, 2001, 2009; Cochran et al., 2004; Tanaka et al., 2002, 2006; Tanaka, 2010, 2012; Thomas et al., 2012). As mentioned by Farrell (1972), an important characteristic of the OTL is its much more irregular distribution, in comparison with the terrestrial tide, which shows smooth variations at the Earth's surface. A detailed theoretical description of ocean tides can be found in e.g. Melchior (1966), Jentzsch (1986, 1997), Zahel (1997), and Agnew (2007).

In Figure 2 we show the components of the strain and radial displacement produced by the OTL effect in the northwestern regions of South America around Colombia and for different major tidal components. As expected, the largest effects are close to the west coast, in the Pacific basin for the M2 and S2 components and around the Caribbean basin for the O1 constituent. Although the radial displacement (~10 mm) is small as compared to the typical total tidal displacement (~200 mm see Figure 6 in Moncayo et al. 2018) event in points at or close to the ocean basins, the OTL strains are comparable to those produced by the solid tides. The OTL effect, as mentioned before, is large for regions at less than ~200 km from the coast.

#### **4. Tidal triggering and the tidal Coulomb failure stress (TCFS)**

The feasibility that tides trigger seismic activity in a given region of the Earth strongly depends on the comparison of the magnitude of the local endogenic (e.g. tectonic) and the external tidal effects. The stresses induced by Earth tides are of the order of  $10^3$  Pa (e.g. Cochran et al., 2004) while those of the OTL can reach values as large as  $10^4$  Pa (e.g. Cochran et al., 2004). Therefore, tidal stresses are 3-4 orders of magnitude smaller than that of tectonic origin. This comparison is one of the main drawbacks of the hypothesis of tidal triggering of seismicity.

However, tidal stress rates can be comparable and even much larger than tectonic stress rates (e.g. Emter, 1997). Assuming, for instance, that OTL stresses build up during half of the semidiurnal cycle, tidal stress rate can be as large as  $\sim 1.7 \times 10^3$  Pa/h (near the coast, the tidal loading signal can overlap the solid tide signal, e.g. Jentzsch, 1997). This value is two orders of magnitude larger than tectonic stress rates  $\sim 17$  Pa/h (Heaton, 1975). Therefore and in contrast to tectonic stress, tidal stress may contribute to activate faults already in a critical state (e.g. Smith and Sammis, 2002; Bucholc and Steacy, 2016). A similar argument has been raised in the case of volcanic regions (Jentzsch et al., 2001).

Even although the critical effect in tidal triggering could be the rate at which stresses are built and not their absolute magnitude, estimating the relative “direction” of the tides with respect to the principal plane of the faults where seismic events arise is critical at evaluating the possible causal relationship between both phenomena.

Estimating tidal stresses is, however, not a trivial matter (Stein, 1999; Vidale et al., 1998; Cochran et al., 2004; Fischer et al., 2006; Wilcock, 2009; Xu et al., 2011; Miguelsanz del Álamo, 2016; Bucholc and Steacy, 2016). In this work we will use the typical approach used by many authors, namely estimating the tidal stress as a linear combination of the normal and shear stress at the fault plane. This “combined stress” is called the Tidal Coulomb Failure Stress (TCFS):

$$\sigma_c = \sigma_s + \mu_f \sigma_n \quad [2]$$

Here  $\mu_f$  is the apparent friction coefficient (King et al., 1994),  $\sigma_n$  is the normal tidal stress, which is considered positive for extension, and  $\sigma_s$  is the tidal shear stress, positive in the slip direction of the fault. Positive values of the TCFS components would be normally associated to fault slip (e.g. Stein, 1999; Galovic et al., 2008; Miguelsanz del Álamo, 2016).

There is no consensus on the best value for  $\mu_f$ . It can be as low as 0.2 and as large 0.8. Several authors, however, have found that a value  $\mu_f = 0.4$  lead to the largest values of the TCFS when a correlation between tides and seismicity seems to exist (e.g. Cochran et al., 2004; Fischer et al., 2006; Bucholc and Steacy, 2016; Miguelsanz del Álamo, 2016).

The value of the normal and shear stresses can be computed from the tidal traction vector,  $\mathbf{T}$ , whose components are defined in terms of the stress tensor  $\sigma_{ij}$  as  $\mathbf{T}_i = \sigma_{ij} \mathbf{n}_j$ , where  $\mathbf{n}$  is a vector normal to the fault plane. Using the traction vector, the normal ( $\sigma_n$ ) and shear ( $\sigma_s$ ) components of the stress are (Xu et al., 2011; Miguelsanz del Álamo, 2016):

$$\sigma_s = \mathbf{T} \cdot \mathbf{s} \quad [3]$$

$$\sigma_n = \mathbf{T} \cdot \mathbf{n} \quad [4]$$

where we have additionally introduced the slip vector  $\mathbf{s}$ .

The normal and slip vectors are given in terms of the parameters of the fault mechanisms, namely the strike ( $\varphi$ ), dip ( $\delta$ ) and rake ( $\lambda$ ), by (Miguelsanz del Álamo, 2016):

$$\mathbf{s} = \begin{pmatrix} \sin \varphi \cos \lambda - \sin \lambda \cos \delta \cos \varphi \\ \cos \lambda \cos \varphi + \sin \lambda \cos \delta \sin \varphi \\ \sin \lambda \sin \delta \end{pmatrix} [5]$$



$$\mathbf{n} = \begin{pmatrix} \cos \varphi \sin \delta \\ -\sin \varphi \sin \delta \\ \cos \delta \end{pmatrix} \quad [6]$$

The constitutive equation for an isotropic material, provide us the relationship between the stress and the components of the strain  $e_{ij}$ :

$$\sigma_{ii} = \lambda e_{kk} + 2\mathcal{G}e_{ii} \quad [7]$$

$$\sigma_{ij} = 2\mathcal{G}e_{ij} \quad [8]$$

Here,  $\lambda$  and  $\mathcal{G}$  are the Lamé coefficients, with  $\mathcal{G}$  the *rigidity* of the material, which for the Earth's crust has values between 30 GPa and 75 GPa (Turcotte and Schubert, 2002). On the other hand, the Lamé coefficient  $\lambda$  is obtained from rigidity  $\mathcal{G}$  and Poisson's ratio  $\nu$  (Stein and Wysession, 2003; Miguelsanz del Álamo, 2016)

$$\lambda = \frac{2\mathcal{G}\nu}{1-2\nu} \quad [9]$$

Combining Eqs. (5-9), the traction vector can be written explicitly as:

$$\mathbf{T} = \boldsymbol{\sigma} \cdot \mathbf{n} = \frac{2\mathcal{G}\nu}{1-2\nu} \begin{bmatrix} ((1-\nu)e_{xx} + \nu(e_{yy} + e_{zz}))(\cos \varphi \sin \delta) - (1-2\nu)e_{xy} \sin \varphi \sin \delta - (1-2\nu)e_{xz} \cos \delta \\ (1-2\nu)e_{xy}(\cos \varphi \sin \delta) - (\nu(e_{xx} + e_{zz}) + e_{yy}(1-\nu)) \sin \varphi \sin \delta + (1-2\nu)e_{yz} \cos \delta \\ (1-2\nu)e_{zx}(\cos \varphi \sin \delta) - (1-\nu)e_{yz} \sin \varphi \sin \delta + ((1-\nu)e_{zz} + \nu(e_{xx} + e_{yy})) \cos \delta \end{bmatrix} \quad [11]$$

here, the strain components  $e_{xx}, e_{yy}, e_{zz}, e_{xy}, e_{yz}, e_{xz}$  are expressed using a local cartesian coordinate system ( $x$  corresponds to east E,  $y$  to north N and  $z$  to the up-direction U) (e.g. Smith and Sammis, 2002; Fischer et al., 2006; Jaeger et al., 2007; Miguelsanz del Álamo, 2016). Explicitly these components are:

$$e_{xx} = \frac{\partial u_x}{\partial x} = e_{EW} \quad \text{Horizontal strain } 90^\circ \quad [12]$$

$$e_{yy} = \frac{\partial u_y}{\partial y} = e_{NS} \quad \text{Horizontal strain } 0^\circ \quad [13]$$

$$e_{zz} = \frac{\partial u_z}{\partial z} = e_{UU} \quad \text{Vertical strain} \quad [14]$$

$$e_{xy} = e_{yx} = e_{NE} - \frac{1}{2}(e_{NS} + e_{EW}) \quad \text{(horizontal tidal shear strain)} \quad [15]$$

$$e_{xz} = e_{zx} = e_{EZ} - \frac{1}{2}(e_{EW} + e_{UU}) \quad [16]$$

$$e_{yz} = e_{zy} = e_{NZ} - \frac{1}{2}(e_{NS} + e_{UU}) \quad [17]$$

In the equations above,  $e_{NE}, e_{EZ}$  and  $e_{NZ}$  are the diagonal strains in the N45E, E45Z and N45Z directions, respectively.

For earthquakes close to Earth's surface we can assume a free surface boundary condition, i.e. the shear strains  $e_{xz}$  and  $e_{yz}$  almost vanish (Harrison, 1976). This

implies  $\sigma_{xz} = \sigma_{yz} = 0$  (Zürn and Wilhelm, 1984). Additionally, we can also assume a state of plane strain, namely  $e_{zz} = 0$ . Both of these assumptions are common when studying shallow earthquakes (e.g. Wilcock, 2009; Smith and Sammis, 2002; Fischer et al., 2006). In this case, the traction vector is finally obtained as:

$$\mathbf{T} = \frac{2G\nu}{1-2\nu} \begin{bmatrix} (1-\nu)e_{xx} + \nu(e_{yy})(\cos\varphi \sin\delta) - e_{xy} \sin\varphi \sin\delta \\ (1-2\nu)e_{xy}(\cos\varphi \sin\delta) - (\nu e_{xx} + e_{yy}(1-\nu)) \sin\varphi \sin\delta \\ \nu(e_{xx} + e_{yy}) \cos\delta \end{bmatrix} \quad [18]$$

Although for the calculation of the tidal stress we need to consider the depth of earthquakes (Tsuruoka et al., 1995), in the case of intermediate-depth earthquakes the previous simplification are still valid. Shear stresses are near zero from Earth's surface to approximately 200 - 300 km depth (Varga and Grafarend, 1996, 2017).

Depending on the sign of the involved stress, the slip of the fault may be favored or not (e.g. Tsuruoka et al., 1995). A positive normal stress means the total normal pressure on the fault decreases and so the slip will be favored (e.g. Miguelsanz del Álamo, 2016; Bucholc and Steacy, 2016). The same happens for the shear stress; if it is positive, it implies that the movement of the fault is favored (Xu et al., 2011).

## 5. TCFS for intermediate depth events in Northwestern South America

In Moncayo et al. (2018) we presented statistical evidences of a positive correlation between tides and seismicity in the Bucaramanga seismic nest and in the Cauca cluster. To actually demonstrate that this correlation anomalies, actually correspond to causal effect (tidal triggering), we need to go further (see e.g. Ader and Avouac, 2013). Here, we will study the problem from a geophysical point of view, computing the tidal stresses acting in several of the earthquake nucleation areas identified in Northwestern South America.

As explained in previous section, this goal requires the estimation of the components of the strain tensor at the place and time of seismic events, besides knowing the detailed geometrical characteristics of the failure where those events arise.

The main inputs for the present study consist of information about seismic events occurred in northwestern South America and time series of solid Earth tides and OTL at the place and time of the selected events.

### 5.1. The selected dataset

For the seismic events within the Bucaramanga nest and Cauca cluster, we used the datasets from the Colombian National Seismological Network (RSNC), managed by the Colombian Geological Survey and freely available online at <http://seisan.sgc.gov.co/RSNC>. The dataset contains 167162 earthquakes recorded from 1993 to 2017. Approximately 70% of the events in the database correspond to intermediate-depth seismic events occurred in the Bucaramanga nest and Cauca

cluster ([Moncayo et al., 2018](#)). The number of events with information about moment tensors and focal mechanisms is however restricted.

We extracted source mechanism information mainly from [Cortes and Angelier \(2005\)](#), which contains events between 1964 and 2002, and from the dataset of the Global Centroid-Moment-Tensor (CMT) catalog from 1997 to 2017 ([Dziewonski et al., 1981](#); [Ekström et al., 2012](#)). This information freely available online at [www.globalcmt.org](http://www.globalcmt.org). Additional information was obtained from [Salcedo et al. \(2001\)](#) and [Tabares et al. \(1999\)](#) both of which contain earthquakes from 1966 to 1992. The focal mechanism of the seismicity in the Puyo and Pucallpa regions was obtained from the CMT catalog for the same time periods mentioned above.

Using the preceding criteria, we select 55 earthquakes of the Bucaramanga nest and 22 of the Cauca cluster, from 1977 to 2017, with information of focal mechanisms. The range of magnitudes for the Bucaramanga and Cauca areas goes from 4.2 to 6.3. Depths for these events range between 120 and 172 km for the Bucaramanga nest, and from 90 to 189 km for the Cauca cluster. The focal mechanisms of the Bucaramanga nest show some variability ([Zarifi and Havskov, 2003](#); [Frohlich et al., 2009](#)), but most of them correspond to reverse mechanisms ([Frohlich et al., 2009](#)). In the supplementary Tables S1 – S4 we show all the events considered in this work with all the parameters of their focal mechanisms.

Additionally, from the CMT catalog we extracted focal mechanisms for 22 earthquakes in the Puyo seismic area, and 28 for the Pucallpa seismic cluster (Supplemental Tables S5 and S8). These earthquakes have magnitudes between 4.9 and 7.0 and depths between 144 and 197 km.

## 5.2. OTL and BT time series computation

Considering the importance of including the OTL effect in the exploration of a relationship between tides and seismicity, we chose the program GOTIC2 ([Matsumoto et al., 2001](#)) to obtain the time series of the indirect effect (OTL) and the joint effect of the solid Earth tides (body tides or BT) and OTL. GOTIC2 ([Matsumoto et al., 2001](#)) is a FORTRAN program, which computes and predicts theoretical BT and OTL in the time domain.

Using GOTIC2 we obtained tidal time series for BT, OTL and the combined effect in a time lapse of 30 days before and after the earthquake. The time series were computed considering the models NAO.99b (global ocean tide model with 0.5° resolution, [Matsumoto et al., 2001](#)) and the long period model NAO.99L ([Takanezawa et al., 2001](#); [Matsumoto et al., 2001](#)), which is a hydrodynamical global model developed using satellite altimetry from 5 years. Both models include 21 tidal constituents: 16 constituents with short period in the diurnal and semidiurnal band (M2, S2, K1, O1, N2, P1, K2, Q1, M1, J1, OO1, 2N2, Mu2, Nu2, L2, T2) and 5 long period constituents (Mtm, Mf, MM, Ssa, Sa).

Although near the coasts it is advisable the usage of combined ocean models of global and regional character (Matsumoto et al., 2001), in our study we use only the global model because most of the analyzed seismic events occurred at a distance larger than 200 km from the coast, where the resolution of the model is enough. A possible improvement of our model will otherwise consider coastal geometry (Jentzsch et al., 2000).

The theoretical OTL effect for the major tidal constituents M2 (principal lunar semidiurnal), S2 (principal solar semidiurnal) and O1 (principal lunar diurnal) is shown for Colombian territory and neighboring regions in Figure 2. The M2 constituent shows the largest amplitude variations, both in the OTL and BT (e.g. Penna et al., 2008). The radial displacement shows its highest values in the Pacific Coast of Colombia for both the semidiurnal principal short period components M2 and S2. The Moon diurnal principal component O1 shows the highest values at the Caribbean Coast. Between M2 and S2 there are differences of one order of magnitude, and between M2 and O1, in some cases the difference reaches two orders of magnitude. If we consider the effect of the OTL on strain, the Moon principal semidiurnal component shows that the tidal effect concentrates in the area of the Pacific Coast for the N-S and E-W components, and the shear strain. In all cases the strain decreases towards the continent, becoming practically negligible at distances larger than 300 km.

### 5.3. TCFS computation

To compute the TCFS we calculated for all the selected events time series of the longitudinal tidal strains for both Earth tides and OTL, as well as the combined effect. Our time series include information about the strain in the north-south, east-west and vertical directions, and in the diagonal direction N45°E. The normal strain components  $e_{yy}$  in north-south direction (also called  $e_{NS}$ ),  $e_{xx}$  in east-west direction (known as  $e_{EW}$ ), the shear component  $e_{xy}$  and the  $e_{zz}$  component were also calculated at the reported place of the event and around the time of occurrence.

In all cases, independently of earthquake depth we use for computing the tidal stresses the criteria of Varga and Grafarend (2017), according to which for depth less than 200-300 km the stress tensor components  $\sigma_{zz}$ ,  $\sigma_{xz}$ ,  $\sigma_{yz}$ ,  $\sigma_{xy}$  are negligible. Additionally we use Green functions in GOTIC2 that were calculated for the surface of the Earth and verified that strains do not differ significantly from those computed with ETERNA 3.40 (Wenzel, 1996, 1997b), which is better suited to compute tidal strains at any depth.

The traction vector, the normal and tangential stresses on the fault plane, were computed using the Cauchy's formula. The latter two would significantly affect fault rupture (e.g. Tanaka et al., 2002; Xie et al., 2015). In all cases, tidal stresses were computed at hypocenter depth, as suggested by Tsuruoka et al. (1995). The normal

and tangential stresses were used to obtain the TCFS of the earthquakes according to Eq. (2).

Following [Cadicheanu et al. \(2014\)](#), we considered all main shock and aftershocks of the intermediate-depth earthquakes in our selected sample. In our previous study ([Moncayo et al., 2018](#)), the whole earthquake database of Colombia was declusterized. However, for the present analysis, the aftershocks are not filtered out. In the case of the Bucaramanga nest, the productivity of the aftershocks has not been reliably detected ([Prieto et al., 2012](#)); additionally, the number of seismic events with information about focal mechanisms for this area is restricted and subtracting possible aftershocks make the statistical analysis tricky. [Prieto et al. \(2012\)](#) suggest that the possible reasons for the limited aftershock productivity are the background seismicity and the lack of events with magnitudes above 6.5. Similar considerations were assumed for the seismic events of the Cauca, Puyo and Pucallpa clusters.

## 6. Results and discussion

The normal and shear stresses computed for all the events in our selected set of earthquakes are presented in Tables S1 and S2 of the supplementary material. From these values, we compute the TCFS using Eq. (2) for at least two different values of the friction coefficient, namely  $\mu_f = 0.2$  and  $\mu_f = 0.4$  and a fiducial rigidity of 75 GPa close to that of the upper mantle ([Turcotte and Schubert, 2002](#)) and more appropriate for intermediate depth earthquakes. Since, from the information provided by the focal mechanisms it is difficult to establish the true nodal plane, we have computed the TCFS for both nodal planes. For each event, these two values of TCFS, are considered as independent events when computing all the statistics presented below.

In Figures 3-7 we plot histograms of the resulting values of the TCFS for the Bucaramanga nest and the Cauca, Puyo and Pucallpa clusters.

We estimate, in all cases, different central momenta of the underlying TCFS distribution: mean, standard deviation, skew and kurtosis. A positive causal relationship is suggested when the mean of the distribution is positive with a standard deviation less or of the same order than the mean. A large positive skew, is also suggestive of a distribution biased towards positive TCFS values. On the other hand, a large positive kurtosis may suggest an underlying distribution which is heavy tailed. The combination of a positive mean, a standard deviation less or of the same order of magnitude, a positive large skew and kurtosis are characteristics favorable to the hypothesis of tidal triggering.

In agreement with previous studies (e.g. [Cochran et al., 2004](#)), a friction coefficient  $\mu_f = 0.4$  tend to produce more positive values of the TCFS than  $\mu_f = 0.2$ .

An interesting effect arises when we compute the TCFS at two different times: 1) at the precise time of the earthquake occurrence (lower panels in Figures 3-7), which

is the most natural election; and 2) at the time of maximum tidal strain just before the time of the earthquake (upper panels in Figures 3-7). We will call the latter the “pre-earthquake time”. The typical difference between these two times is of a few hours and never is larger than 12 hours (the time between semidiurnal peaks). The calculation of the TCFS before the events, is aimed at testing the hypothesis that the tidal triggering could not be instantaneous.

It is interesting to notice that although the TCFS values at the time of maximum tides before the event, are not too much larger than the values at the time of earthquakes, they are significantly more biased towards positive values. This result is more evident in the box plots of Figure 8 and the scatter plots in Figures 9 and 10.

This trend suggests that tidal triggering is not instantaneous, but it could build up before the occurrence of the earthquake in such a way that at the time of the earthquake the fault could have already relaxed enough to generate the event.

In the following paragraphs we analyse the results for each studied area.

### **6.1. Bucaramanga**

The statistics of the TCFS calculated for the Bucaramanga seismic nests are in Figures 3, 8 (upper-left panel), 9, 10, 11.

As mentioned before a large friction coefficient is more consistent with the hypothesis of tidal triggering. When the pre-earthquake strains are calculated, we find a positive average TCFS value with a dispersion of the same order than the average (Figure 3, upper-right panel). In this case, also the skewness and the kurtosis are positive, which is also consistent with delayed tidal triggering.

The box plots in Figure 8 confirm these conclusions. We see that when using the pre-earthquake strain (upper-left panel, left box), the median of the TCFS values are well above zero. Intriguingly, the TCFS values computed at the time of earthquakes have an excess of atypical values at both sides of zero.

More interestingly are the scatter plots in Figures 9, showing the correlation between the phase of the earthquakes as computed in Moncayo et al. (2018) for the two components where they found correlation anomalies, and the value of the TCFS. The asymmetry in the distribution of the TCFS values is evident in these plots, reinforcing the previous conclusions. However, the more interesting feature is the dependency of TCFS distribution on the value of the phase. Thus, for instance, for the monthly tidal phase, negative TCFS values are only common for values around 0.5, while positive TCFS values are dominant for values of the phase close to 0 and 1. This is precisely what was expected from the correlation anomalies observed in Moncayo et al. (2018).

According to Curchin and Pennington, (1987), the Bucaramanga nest does not show a relationship between the semidiurnal tides and the earthquake origin time; however, they do not include the monthly phase in their calculation, which is the one

that more strongly suggests the effect of the tide to facilitate the slip along the fault planes defined by the focal mechanism.

Consistent with the “delayed triggering” hypothesis are the scatter plots in Figure 10, where no preferred sign of the TCFS, nor strong TCFS-phase correlations are observed.

## **6.2. Cauca**

The statistics of the TCFS calculated for the Cauca cluster are in Figures 4, 5 and 8 (upper-right panel).

If we consider only the effect of the body tides, BT for short (Figures 4), no significant asymmetry in the TCFS values are observed, nor at the time of the earthquakes or at pre-earthquake times. However, when both BT and the ocean tidal loading (OTL) are considered (Figure 5) a similar picture as that observed in the Bucaramanga seismic nests, arises. At pre-earthquake times, large average values of TCFS with a dispersion of the same order than the average and a skewed distribution, are observed in this region. This result shows how important could be the inclusion of the OTL effects, especially in regions not too far from the coast, when studying tidal triggering.

The results in Figure 5 for the Cauca cluster, is confirmed in the box diagrams in the upper-right panel of Figure 8. The significant bias of TCFS for events in this area toward positive values, is even more significant than in the case of the Bucaramanga seismic nest.

## **6.2. Puyo and Pucallpa**

The statistics of the TCFS calculated for the Puyo and Pucallpa clusters are in Figures 6, 7 and 8 (lower row).

Considering the TCFS calculated at the time of maximum strain before the earthquake, and using friction coefficients of 0.2 and 0.4 and a rigidity of 75 Gpa (Figures 6 a, b and 7 a, b), we observe consistently positive values of TCFS with a average near 1000 Pa. In these areas, the average TCFS calculated at pre-earthquake is larger than the dispersion, in contrast with the case of the Bucaramanga an Cauca regions. The skewness of the distribution of TCFS values are also very large.

The statistics for this regions represented in the box plots of Figure 8 confirms again the trend observed in Bucaramanga and Cauca.

If we consider the positive values of the TCFS obtained for the four seismic clusters, and we analyze the type of fault associated with the focal mechanisms, we can observe that they mostly correspond to strike slip with some dip slip (reverse). This could mean that the gravitational effect of the Moon and the Sun could provide a loosening effect in this type of faults, which could facilitate sliding. This result, despite

the small number of data, would be in agreement with results reported by Bucholz and Steacy (2016) and Miguelsanz del Álamo (2016) in California.

Frohlich et al. (2009) mention some studies that consider dehydration embrittlement as one of the most accepted explanations for the occurrence of intermediate-depth earthquakes. They suggest that the intermediate-depth earthquakes occur within cold and stressed subducted lithosphere. The confining pressures to the hypocenter depth for the Bucaramanga nest earthquakes could be near 4 GPa, and as Frohlich et al. (2009) mentioned, the periodic tidal stresses are too small (near three orders of magnitude) to cause rupture at these pressures. However, it must be kept in mind the existence of tidal stress rates that could be larger (Emter, 1997). Puyo and Pucallpa seismic nests are other places where there might be a favorable tendency for the tidal triggering of earthquakes (Figures 6 and 7); an initial exploration was performed, but a study with a larger database is needed in future investigations.

## **7. Summary and Conclusions**

Although a small number of events with focal mechanism information for the selected seismic clusters were available (55 for Bucaramanga, 22 for Cauca, 22 for Puyo, and 28 for Pucallpa), the results of our calculation of TCFS show favorability of tidal triggering of earthquakes.

Since the Bucaramanga nest was the one with the greatest event sample and the clearest connection between tides and seismicity, we performed additional tests to elucidate how such a connection may work. According to our results, there is no global marked correlation between the values of TCFS and the vertical strain for the monthly and diurnal phases; however, a slight correlation for the monthly phase at the earthquake origin time is hinted by the data. The TCFS seems to favor the earthquake nucleation during the second half of the lunar cycle, when the Earth and the Moon are approaching each other; this fact enforces the hypothesis that the tidal monthly phase is the one that more actively contributes to earthquake nucleation in the Bucaramanga nest.

Our statistical results suggest that in general tidal forcing may contribute to trigger earthquakes at seismic clusters of intermediate depth. However, there is no definitive and global evidence for this effect, and according to our results, it could be that the role of tidal stresses is different for every nest. Future investigations with larger data sets will contribute to clarify this situation.

## **Acknowledgements**

G.Moncayo wants to thank the Administrative Department of Science, Technology and Innovation of Colombia COLCIENCIAS, for their financial support during the year 2016. Many thanks to Dr. Thomas Jahr and PhD Student Chris Salomon from the Institute of Geosciences of the Friedrich-Schiller University (FSU) of Jena



(Germany), for the useful discussions and support during the 3-month internship of G. Moncayo at this University (September to December 2016); as well as to Dr. Adelheid Weise (LIAG-Leinbniz Germany) and Prof. i.R. Dr. Gerhard Jentzsch (FSU) Jena for the useful recommendations in relation with this work. Additionally, many thanks to Dr. Walter Zuern from Black Forest Observatory (Germany), Dr. Kogi Matsumoto (National Astronomical Observatory-japan, GOTIC2 program) for the personal communications, and to Jorge Castro at the Mariana University in Pasto for the support with some statistical suggestions for the work. Discussions with Dr. Ludger Suarez from the National University of Colombia greatly helped to encourage and improve this research.

We thank the Colombian Geological Survey and the National Seismological Network of Colombia (RSNC), for the free available earthquake database and some personal communications. We thank the Global Centroid Catalog too, for the free accessibility to focal mechanism information.

## References

Arabelos et al., 2016. D.N. Arabelos, M. E. Contadakis, G. Vergos and S. Spatalas. Variation of the Earth tide-seismicity compliance parameter during the recent seismic activity in Fthiotida, central Greece. *Annals of Geophysics*, 59, 1 (2016), S0102; doi: 10.4401/ag-6795.

Ader et al., 2013. T.J. Ader and J.P. Avouac. Detecting periodicities and declustering in earthquake catalogs using the Schuster spectrum, application to Himalaya seismicity. *Earth and Planet. Sci.Lett.* 377-378 (2013) 97-105. [http://dx.doi: 10.1016/j.epsl.2013.06.032](http://dx.doi.org/10.1016/j.epsl.2013.06.032).

Agnew 2007. D. C. Agnew. *Earth Tides*. University of California San Diego. Elsevier (2007).

Baker, 1984. T. F. Baker, 1984. Tidal deformations of the Earth. *Sci. Prog. Oxf.* 69 No. 274 (1984) 197-233.

Barazangi and Isacks ,1976. M. Barazangi and B.L. Isacks. Spatial distribution of earthquakes and subduction of the Nazca plate beneath South America. *Geology* V. 4, (1976) 686-692.

Bucholc and Steacy, 2016. M. Bucholc and S. Steacy. Tidal stress triggering of earthquakes in Southern California. *Geophys. J. Int.* (2016), doi: 10.1093/gji/ggw045.

Cadicheanu et al., 2007. N. Cadicheanu, M. van Ruymbeke, and P. Zhu. Tidal triggering evidence of intermediate depth earthquakes in the Vrancea zone (Romania). *Nat. Hazards Earth Syst. Sci.*, 7 (2007) 733–740. <hal-00299472>

Cadicheanu et al., 2014. N. Cadicheanu, M. van Ruymbeke, and P. Zhu. On the variability of the coupling between some earth tide periodicities and earthquake triggering from three important seismic nest regions on Earth. Available at [http://www.eas.slu.edu/GGP/BIM\\_Recent\\_Issues/bim%20148-2014/cadicheanu\\_etal\\_coupling\\_tides\\_earthquakes\\_BIM148.pdf](http://www.eas.slu.edu/GGP/BIM_Recent_Issues/bim%20148-2014/cadicheanu_etal_coupling_tides_earthquakes_BIM148.pdf).

Cardona et al., 2005. Cardona C., Salcedo E. de J., Mora, H. Caracterización Sismotectónica y Geodinámica de la Fuente Sismogénica de Murindó-Colombia. *Boletín de Geología*, Vol. 27, No. 44 (2005) 115-132.

Chang et al., 2017. Y. Chang, L.M. Warrior and G. Prieto. Precise Locations for Intermediate-Depth Earthquakes in the Cauca Cluster, Colombia. *Bull. Seismol. Soc. Am.* (2017) 107 (6): 2649-2663, doi: 10.1785/0120170127

Chiarabba et al., 2015. C. Chiarabba, P. De Gori, C. Faccenna, F. Speranza, D. Seccia, V. Dionicio and G. Prieto. Subduction system and flat slab beneath the Eastern Cordillera of Colombia. *Geochem. Geophys. Geosyst.*, 16 (2015), 17-27, doi: 10.1002/2015GC006048.

Cochran et al., 2004. E.S. Cochran, J.E. Vidale & S. Tanaka. Earth Tides can Trigger Shallow Thrust Fault Earthquakes. *Science*, 306 (2004), doi: 10.1126/Science.1103961.

Cortes and Angelier, 2005. M. Cortés & J. Angelier. Current states of stress in the northern Andes as indicated by focal mechanisms of earthquakes. *Tectonophysics* 403 (2005) 29-58, doi:10.1016/j.tecto.2005.03.020.

Curchin and Pennington, 1987. J.M. Curchin and W.D. Pennington. Tidal triggering of Intermediate and Deep Focus Earthquakes. *J. Geophys. Res.*, 92 B13 (1987) 13957-13967.

Doan et al., 2006. M.L. Doan, E. Brodsky, R. Prioul and C. Signer. Tidal analysis of borehole pressure. A tutorial. Schlumberger-Doll Research Report, (2006) Santa Cruz University of California.

Dziewonski et al., 1981. Dziewonski, A. M., T.-A. Chou and J. H. Woodhouse. Determination of earthquake source parameters from waveform data for studies of global and regional seismicity. *J. Geophys. Res.*, 86, (1981) 2825-2852, doi:10.1029/JB086iB04p02825.

Eakin et al., 2014. C.M. Eakin, M.D. Long, S.L. Beck, L.S. Wagner, H. Tavera and C. Condori. Response of the mantle to flat slab evolution: Insights from local S splitting beneath Peru. *Geophys. Res. Lett.*, 41 (2014) 3438-3446, doi:10.1002/2014GL059943.

Emter, 1997. D. Emter. Tidal Triggering of Earthquakes and Volcanic Events. Tidal Phenomena, Lecture Notes in Earth Science, 66 (1997) 293-309.

Ekström et al 2012. Ekström, G., M. Nettles, and A. M. Dziewonski. The global CMT project 2004-2010: Centroid-moment tensors for 13,017 earthquakes. Phys. Earth Planet. Inter., (2012) 200-201, 1-9, doi:10.1016/j.pepi.2012.04.002.

Farrell, 1972. W.E. Farrell. Deformation of the Earth by surface loads. Rev. Geophys. Space. Phys., 10 No. 3 (1972) 761-797.

Farrell, 1973. W.E. Farrell. Earth Tides, Ocean Tides and Tidal Loading. Phil. Trans. R. Soc. Lond. A 274 (1973) 253-259, doi: 10.1098/rsta.1973.0050.

Fedotov, 1965. S.A. Fedotov. Regularities of the distribution of strong earthquakes in Kamchatka, the Kurile Islands and northeastern Japan (in Russian). Tr. Inst. Fiz. Zemli Akad. Nauk SSSR 36(203) 66-93.

Fischer et al., 2006. T. Fischer, P. Kalenda and L. Skalsky. Weak tidal correlation of NW-Bohemia/Vogtland earthquake swarms. Tectonophysics 424 (2006) 259-269, doi:10.1016/j.tecto.2006.03.041.

Frolich et al., 2009. C. Frolich and Y. Nakamura. The physical mechanisms of Deep moonquakes and intermediate-depth earthquakes: How similar and how different?. Phys. Earth and Planet. Int. 173 (2009) 365-374, doi:10.1016/j.pepi.2009.02.004.

Gallego et al., 2013. A. Gallego, R.M. Russo, D. Comte, V. Mocanu, R.E. Murdic and J.C. Van Decar. Tidal modulation of continuous nonvolcanic seismic tremor in the Chile triple junction region. Geochem. Geophys. Geosyst, 14 (2013) 851-863, doi. 10.1002/ggg2.20091.

Gallovic, 2008. F. Gallovic. Heterogeneous Coulomb stress perturbation during earthquakes cycles in a 3D rate-and-state fault model. Geophys. Res. Let. 35 (2008) L21306, doi: 10.1029/2009GL035614.

Gansser, 1973. A. Gansser. Facts and theories on the Andes. J. Geol. Soc. 129 (1973) 93-131.

Gutscher et al., 2000. M.A. Gutscher, W. Spakman, H. Bijwaard and E.R. Engdahl. Geodynamics of flat subduction: Seismicity and tomographic constraints from the Andean margin. Tectonics Vol. 19 No. 5 (2000) 814-833.

Harrison, 1976. J. C. Harrison. Cavity and Topographic Effects in Tilt and Strain Measurement. J. Geophys. Res., 81 (2) (1976) 319-328.

Heaton, 1975. T. Heaton. Tidal Triggering of Earthquakes. Geophys. J.R. ast. Soc., 43 (1975) 307-326.

Idarraga-García et al., 2016. J. Idarraga-Garcia, J.-M. Kendall and C.A. Vargas. Shear wave anisotropy in Northwestern South America and its link to the Caribbean and Nazca subduction geodynamics. *Geochem., Geophys., Geosyst.* Doi 10.1002/2016GC006323.

Jaeger et al., 2007. J. C. Jaeger, N. G. Cook and R. W. Zimmerman. *Fundamentals of Rock Mechanics*. Fourth Edition, Blackwell Publishing (2007).

Jentzsch, 1986. G. Jentzsch. *Auflastgezeiten in Fennoskandien*. Berliner Geowissenschaftliche Abhandlungen Reihe B/Band 13 Geophysik. Dietrich Reimer Verlag in Berlin (1986) 184. ISBN 3-469-00265-4.

Jentzsch, 1997. G. Jentzsch. Earth tides and ocean tidal loading. In: Wilhelm, H., Zürn, W. Wenzel, H.G. (Ed), *Tidal Phenomena. Lecture Notes in Earth Science*, 66 (1997) 145-171, doi: 10.1007/BFb0011461

Jentzsch et al., 2000. G. Jentzsch, P. Knudsen and M. Ramatschi, 2000. Ocean Tidal Loading Affecting Precise Geodetic Observations on Greenland: Error Account of Surface Deformations by Tidal Gravity Measurements. *Phys, Chem, Earth (A)*, 25 (2000) 401-407.

Jentzsch et al., 2001. G. Jentzsch, O. Haase, C. Kroner, U. Winter. Mayon volcano, Philippines: some insights into stress balance. *J. Volcanol. Geoth. Res.*, 109 (2001) 205-217, doi: 10.1016/S1464-1985(00)00063-3.

King et al., 1994. G.C.P. King, R.S. Stein and J. Lin. Static Stress Changes and the Triggering of Earthquakes. *Bull. Seismol. Soc. Am.* 84 No. 3 (1994) 935-953.

Matsumoto et al., 2001. K. Matsumoto, T. Sato, T. Takanezawa and M. Ooe. GOTIC2: A Program for Computation of Oceanic Tidal Loading Effect. *J. Geod. Soc. Japan*, 47 No. 1 (2001), pp. 243-248.

Melchior, 1966. P. Melchior. *The Earth Tides*. Oxford (1966) 458 p.

Métivier et al., 2009. L. Métivier, O. de Viron, C.P. Conrad, S. Renault, M. Diament, G. Patau. Evidence of earthquake triggering by the solid earth tides. *Earth Planet. Sc. Lett.*, 278 (2009), pp. 370-375, doi:10.1016/j.epsl.2008.12.024.

Miguelsanz del Álamo, 2016. L. Miguelsanz del Álamo. *Relaciones entre mareas y otros fenómenos geodinámicos: estudios en la Península Ibérica y California*. Tesis inédita de la Universidad Complutense de Madrid, Facultad de Ciencias Matemáticas, Sección Departamental de Astronomía y Geodesia.

Moncayo et al., 2018. G.A. Moncayo; J. I. Zuluaga and G. Monsalve Mejía. Correlation between tides and seismicity in Northwestern South America: the case of Colombia. In revision. Available at ArXiv repository: 1804.07235

Penna et al., 2008. N.T. Penna, M.S. Bos, T.F. Baker and H.G. Schernek. Assessing the accuracy of predicted ocean tide loading displacement values. *J. Geod.*, 82 (2008), pp. 893-907, doi: 10.1007/s00190-008-0220-2.

Pennington, 1981. W. D. Pennington. Subduction of the Eastern Panama Basin and Seismotectonics of Northwestern South America. *J. Geophys. Res.* 86, NO. B11 (1981) 10753-10770, doi: 10.1029/JB086iB11p10753.

Prieto, et al., 2012. G. Prieto, G. Beroza, S.A. Barret, G.A. López & M. Flórez. Earthquakes nest as natural laboratories for the study of intermediate-depth earthquakes mechanics. *Tectonophysics* 570-571 (2012) 42-56, doi.org/10.1016/j.tecto.2012.07.019

Pulido, 2003. N. Pulido. Seismotectonics of the Northern Andes (Colombia) and the development of seismic networks. *B. Int. Inst. Seismol. Earthq. Eng.*, (2003) 69-76 Special Edition.

Ramos, 1999. V.A. Ramos. Plate tectonic setting of the Andean Cordillera. *Episodes* Vol. 22 No.3 (1999) 183-190.

Ramos and Kay, 1992. V.A. Ramos and Kay. Southern Patagonian plateau basalts and deformations: backarc testimony of ridge collisions. *Tectonophys.* 205 (1992) 261-282, doi: 10.1016/0040-1951(92)90430-E.

Salcedo et al., 2001. E.J. Salcedo Hurtado., C.I. Rivera Pérez and A. A. Gómez C. Implicaciones sismotectónicas de las soluciones del mecanismo focal de algunos terremotos de la región central de Colombia. *Geofísica Colombiana* No. 5 (2001) 18-26.

Sanchez-Rojas and Palma, 2014. J. Sanchez-Rojas and M. Palma. Crustal density structure in northwestern South America derived from analysis and 3-D modeling of gravity and seismicity data. *Tectonophysics* 634 (2014) 97-115, doi.org/10.1016/j.tecto.2014.07.026 .

Scherneck, 2001. H. G. Scherneck. Äspö Hard Rock Laboratory. Using borehole tides to determine fracture parameters (1). Chalmers University of Technology, Schweden 2001.

Schneider and Sacks, 1988. J. F. Schneider and I. S. Sacks. Spatial distribution and b-value of intermediate-depth earthquakes beneath Central Peru. *Geophys. Res. Lett.* 15 (12) (1988) 1421-1424, doi: 10.1029/GL05i012p01421.

Sella et al., 2002. G. F. Sella, T. H. Dixon and A. Mao. REVEL: A model for Recent plate velocities from space geodesy. *J. Geophys. Res.* 107, NO. B4 (2002) 2081, doi: 10.1029/2000JB000033, 2002

Smith and Sammis, 2002. S. W. Smith and C. G. Sammis. Revisiting the Tidal Activation of Seismicity with a Damage Mechanism and Friction Point of View. 3rd ACES Workshop Proceedings, Mani, Hawaii 327-332.

Soles Valdivia, 2012. A.M. Soles Valdivia. Sismicidad, esfuerzos y geometría del enjambre sísmico de Pucallpa (Perú). Tesis en español. Master 2SG Ciencias y Gestión de la Tierra, Geología, Riesgos y Gestión del Territorio. Université Nice Sophia Antipolis- Programa PREFALC, Perú (2012) 102 p.

Stein, 1999. R. S. Stein. The role of stress transfer in earthquake occurrence. *Nature* 402 (1999) 605-609.

Stein and Wysession, 2003. S. Stein and M. Wysession. *An Introduction to Seismology, Earthquakes, and Earth Structure*. Blackwell Publishing Ltd. (2003).

Syracuse et al., 2016. M. E. Syracuse, M. Maceira, G. Prieto, H. Zhang and C. Ammon. Multiple plates subducting beneath Colombia, as illuminated by seismicity and velocity from the joint inversion of seismic and gravity data. *Earth and Planetary Science Letters* 444 (2016) 139–149, doi.org/10.1016/j.epsl.2016.03.050.

Tabares et al., 1999. L.M. Tabares Ocampo, H. Mora Páez & E. Salcedo Hurtado. Actividad sísmica y tasa de deformación sismotectónica en la zona del viejo Caldas, Colombia. *Revista Academia Colombiana de Ciencias*. Vol. XXIII, No. 88 (1999) 359-373.

Taboada et al., 1998. A. Taboada, C. Dimaté, A. Fuenzalida. Sismotectónica de Colombia: deformación continental activa y subducción. *Física de la Tierra*, 10 (1998) 111-147. ISSN: 0214-4557.

Taípe Acosta, 2013. L.M Taípe Acosta. Análisis de las ecuaciones de predicción de movimientos de suelo para el Ecuador utilizando datos registrados durante el periodo 2000-2011 en estaciones sísmicas de banda ancha y acelerógrafos. Tesis Escuela Politécnica Nacional-Escuela de Ingeniería Geológica, Quito (2013) 129 p.

Takanezawa et al., 2001. T. Takanezawa, K. Matsumoto, O. Masatsugu and I. Naito. Effects of the Long-Period Ocean Tides on Earth Rotation, Gravity and Crustal Deformation Predicted by Global Barotropic Model – Periods from Mtm to Sa –. *J. Geod. Soc. Japan* 47 No. 1 (2001) 545-550, doi: 10.1136/sokuchi1954.47.545.

Tanaka et al., 2002. S. Tanaka, M. Ohtake, H. Sato. Evidence for tidal triggering of earthquakes as revealed from statistical analysis of global data. *J. Geophys. Res.* 107 (B10) (2002), 2211, doi:10.1029/2001JB001577.

Tanaka et al., 2004. S. Tanaka, M. Ohtake, H. Sato. Tidal triggering of earthquakes in Japan related to the regional tectonic stress. *Earth Planets Space*, 56 (2004) 511-515, doi: 10.1186/BF03352510.

Tanaka et al., 2006. S. Tanaka, H. Sato, S. Matsumura, M. Ohtake. Tidal triggering of earthquakes in the subducting Philippine Sea plate beneath the locked zone of the plate interface in the Tokai region, Japan. *Tectonophysics*, 417 (2006) 69-80, doi:10.1016/j.tecto.2005.09.013.

Tanaka, 2010. S. Tanaka. Tidal triggering of earthquakes precursory to the recent Sumatra megathrust earthquakes of 26 December 2004 (Mw =9.0), 28 March 2005 (Mw = 8,6), and 12 September 2007 (Mw = 8,5). *Geophys. Res. Lett.*, 37 (2010), L02301, doi:10.1029/2009GL041581.

Tanaka, 2012. S. Tanaka. Tidal triggering of earthquakes prior to the 2011 Tohoku-Oki earthquake (Mw 9.1). *Geophys. Res. Lett.*, 39 (2012), L00G26, doi: 1029/2012GL0551179.

Tavera and Buforn, 2001. H. Tavera and E. Buforn. Source mechanism of earthquakes in Peru. *J. of Seismol.* 5 (2001) 519-539, doi: 10.1023/A1012027430555.

Tiwari and Chamoli, 2014. R. K. Tiwari & A. Chamoli. Is tidal forcing critical to trigger large Sumatra earthquakes?. *Nat. Hazards*, (2014), doi: 10.1007/s11069-014-1068-9, doi: 10.1007/s11069-014-1068-9.

Thomas et al., 2012. A.M. Thomas, R. Bürgmann, D.R. Shelly, N.M. Beeler and M.L. Rudolph. Tidal triggering of low frequency earthquakes near Parkfield, California: Implications for fault mechanics within the brittle-ductile transition. *J. Geophys. Res.*, 117 (2012), B05301, doi: 10.1029/2011JB009036.

Trenkamp et al., 2002. R. Trenkamp, J. N. Kellog, J. T. Freymueller & H. P. Mora. Wide plate margin deformation, southern Central America and northwestern South America, CASA GPS observations. *J. South Am. Earth Sci.*, 15 (2002) 157-171, doi: 10.1016/S0895-9811(02)0018-4.

Tsuruoka et al., 1995. H. Tsuruoka, M. Ohtake & H. Sato. Statistical test of the tidal triggering of earthquakes: contribution of the ocean tide loading effect. *Geophys. J. Int.* 122 (1995) 183-194, doi: 10.1111/j.1365-246X.1995.tb03546.x.

Turcotte and Schubert, 2002. D. Turcotte and G. Schubert. *Geodynamics*. Cambridge University Press (2002).

Van der Hilst and Mann, 1994. R. Van der Hilst and P. Mann. Tectonic implications of tomographic images of subducted lithosphere beneath northwestern South America. *Geology* (1994) 22 (5): 451-454, doi 10.1130/0091-7613(1994).

Varga and Grafarend, 1996. P. Varga and E. Grafarend. Distribution of the lunisolar tidal elastic stress tensor components within the Earth's Mantle. *Phys. Earth Planet. Int.* 93 (1996) 285-297, doi: 10.1016/0031-9201(95)03067-0.

Varga and Grafarend, 2017. P. Varga and E. Grafarend. Influence of Tidal Forces on the Triggering of Seismic Events. *Pure Appl. Geophys.* Springer International Publishing (2017), doi 10.1007/s0024-017-1563-5.

Vargas and Mann, 2013. C. A. Vargas and P. Mann. Tearing and Breaking Off of Subducted Slabs as the Result of Collision of the Panama Arc-Indenter with Northwestern South America, *Bull. Seism. Soc. Am.*, 103(3) (2013) 2025-2046, doi: 10.1785/0120120328.

Vidale et al., 1998. J.E. Vidale, D.C. Agnew, M.J. Johnston, D.H. Oppenheimer. Absence of earthquake correlation with Earth tides: An indication of high preseismic fault stress rate. *J. Geophys. Res.*, 103(B10) (1998) 24567-24572, doi:10.1029/98JB00594.

Wendt, 2004. A. Wendt. Untersuchung zu gezeitenbedingten Höhenänderung des subglazialen Lake Vostok, Antartika. Fakultät für Forst-, Geo- und Hydrowissenschaften der Technischen Universität Dresden (2004), Tesis doctoral 128 p.

Wenzel, 1996. H.G. Wenzel. The Nanogal Software: Earth Tide Data Processing Package ETERNA3.30. *BULL. D.INF. Maree Terr.* 124 (1996) 9425-9439.

Wenzel, 1997b. H.G. Wenzel. Earth Tide Data Processing Package ETERNA Version 3.40 Manual ETERNA34.HLP. Black Forest Observatory Universität Karlsruhe, 1997.

Wilcock, 2001. W. Wilcock. Tidal triggering of earthquakes of microearthquakes on the Juan de Fuca Ridge. *Geophys. Res. Let.* 28 (2001) No. 20, 3999-4002, doi/10.1029/2001GL013370.

Wilcock, 2009. W. Wilcock. Tidal triggering of earthquakes in the Northeast Pacific Ocean. *Geophys. J. Int.* (2009) 179, 1065-1070, doi: 10.1111/j.1365-246X.2009.04319.x.

Xu et al., 2011. Y J Xu, X P Wu, C H Yan, Y Huang, Y Wang and L Tao. The Tidal Coulomb Failure Stresses on various kinds of seismic fault. *Chinese J. Geophys.* 54 No. 2 (2011) 197-206.

Yarce et al., 2014. J. Yarce, G. Monsalve, T.W. Becker, A. Cardona, E. Poveda, D. Alvira and O. Ordoñez-Carmona. Seismological observations in Northwestern South America: Evidence for two subduction segments, contrasting crustal thicknesses and upper mantle flow. *Tectonophysics*, 637 (2014), 57-67, doi.org/10.1016/j.tecto.2014.09.006.

Zahel, 1997. W. Zahel. Ocean Tides. In: Wilhelm, H., Zürn, W. Wenzel, H.G. (Ed), *Tidal Phenomena. Lecture Notes in Earth Science*, 66 (1997) 113-143, doi: 10.1007/BFb0011460.



Zahran et al., 2005. K.H. Zahran, G. Jentzsch, G. Seeber. World-wide synthetic tide parameters for gravity and vertical and horizontal displacements. *J. Geod.*, 79 (2005) 293-299, doi 10.1007/s00190-005-0460-3.

Zarifi and Havskov, 2003. Z. Zarifi and J. Havskov. Characteristics of dense nests of deep and intermediate-depth seismicity. *Adv. Geophys.*, 46 (2003) 237-278, doi: 10.1016/S0065-2687(03)46004-4.

Zarifi et al., 2007. Z. Zarifi, J. Havskov and A. Hanyga. An insight into the Bucaramanga nest. *Tectonophysics* 443 (2007) 93-105, doi:10.1016/j.tecto.2007.06.004.

Zürn and Wilhelm, 1984. Zürn W., Wilhelm H. Geophysics of the Solid Earth, the Moon and the Planets. 2.5.2 Tides of the Solid Earth. In: Fuchs K., Soffel H. (eds) Subvolume A. Landolt-Börnstein - Group V Geophysics, vol 2a. (1984) Springer, Berlin, Heidelberg, doi: 10.1007/b20010.

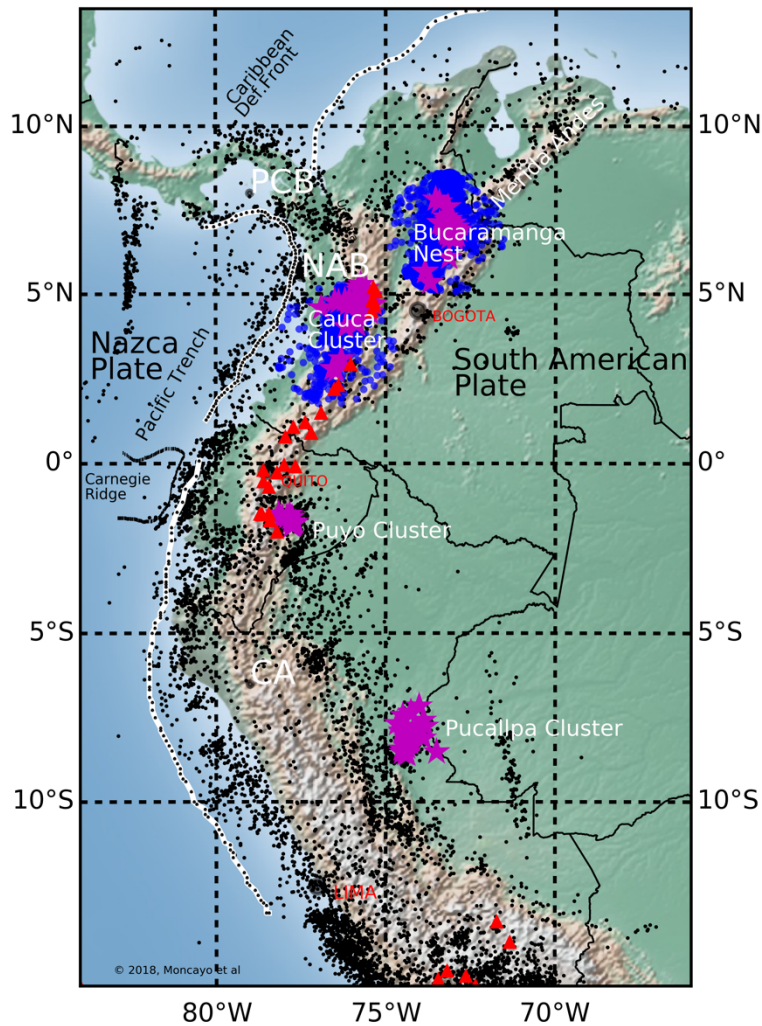


Figure 1. The North Andean Block and the Central Andes (NAB and CA respectively). Black dots show the seismic activity in the region, obtained from the National Earthquake Center (NEIC) and from the Centroid Moment Tensor catalog (CMT), between 1993 and 2018. Blue circles represent all the reported seismic events in the Cauca seismic cluster and in the Bucaramanga seismic nest, considering a radius of 200 km around the center of each nest (lat. 4.5°N, long. 76°W and lat. +7°N, long. 73°W, respectively) and a depth greater than 100 km. Magenta stars correspond to the seismic events with focal mechanism information in the Bucaramanga nest, and the Cauca, Puyo and Pucallpa clusters. Red triangles represent volcanoes. PCB: Panama-Choco Block, NAB: North Andean Block, CA: Central Andes, Caribbean Def. Front: Caribbean Deformation Front.

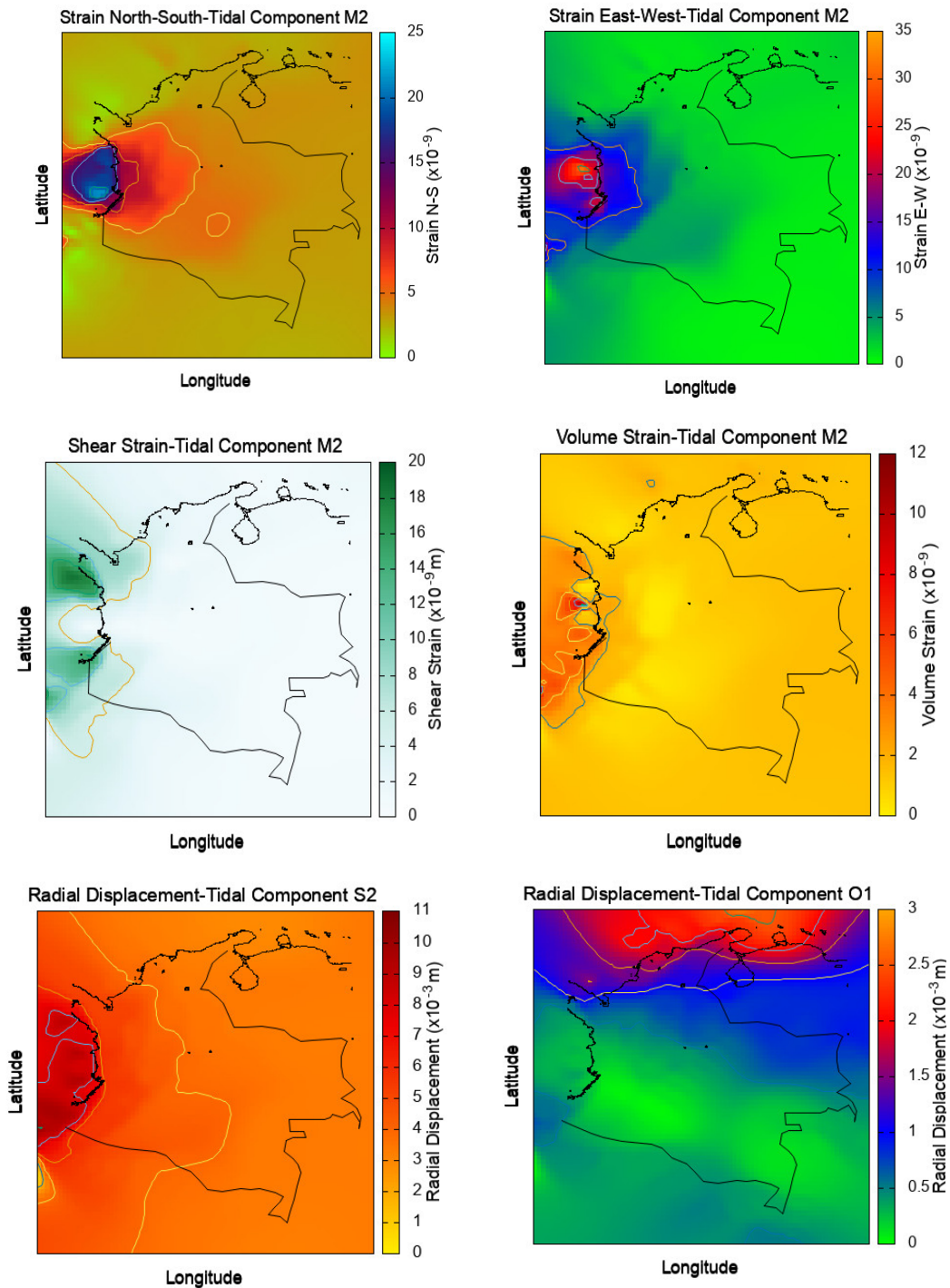


Figure 2. First and second row: OTL strain components (North-South, East-West, shear and volumetric) for Colombian territory and neighboring regions in Northern South America. We plot, for reference, only the strain components for the tidal constituent M2 (principal lunar semidiurnal). Lower row: OTL radial displacement for the short period tidal constituents S2 (principal solar semidiurnal) and O1 (lunar declinational diurnal).

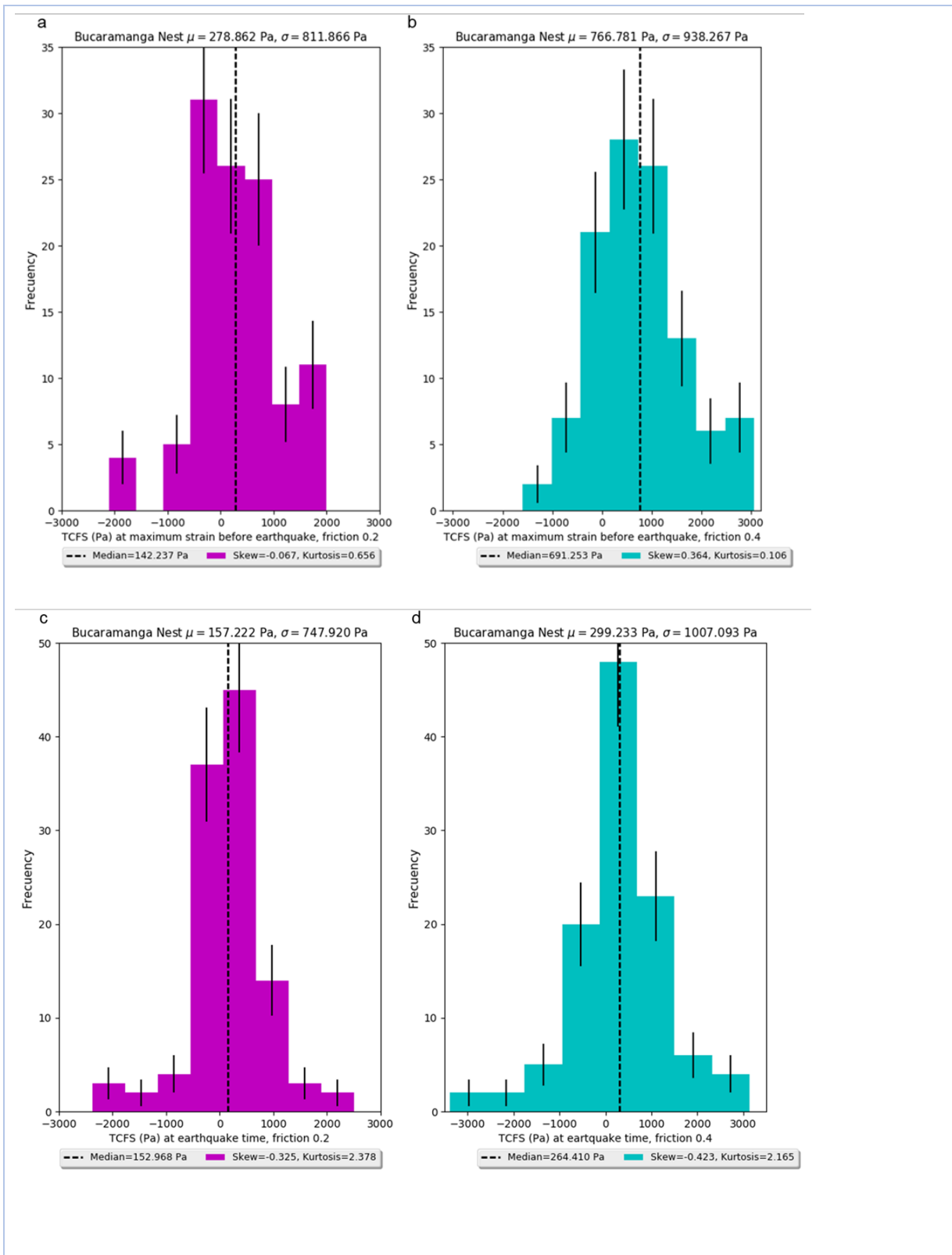


Figure 3. Frequency histograms of the TCFS for the Bucaramanga seismic nest. (a) and (b) show the TCFS calculated at the time of maximum strain before the earthquake occurrence, with friction coefficients of 0.2 and 0.4 respectively. (c) and (d) show the TCFS calculated from tidal strain data at the earthquake origin time, with friction coefficients of 0.2 (c) and 0.4 (d). The histograms include

information of the solid Earth tides and OTL on both possible nodal planes per earthquake, and the rigidity is assumed to be 75 GPa. On top of each histogram we report the mean and standard deviation.

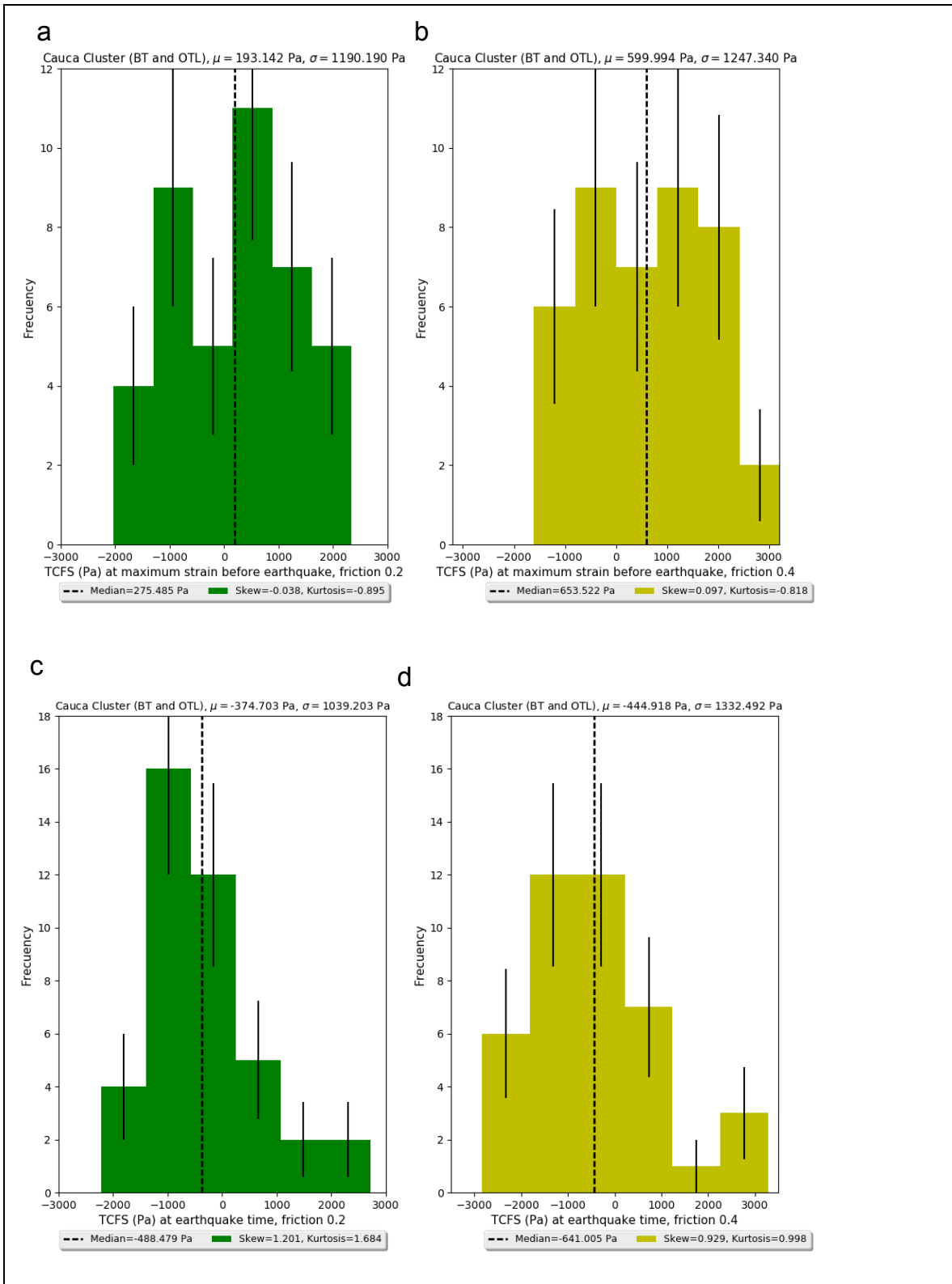
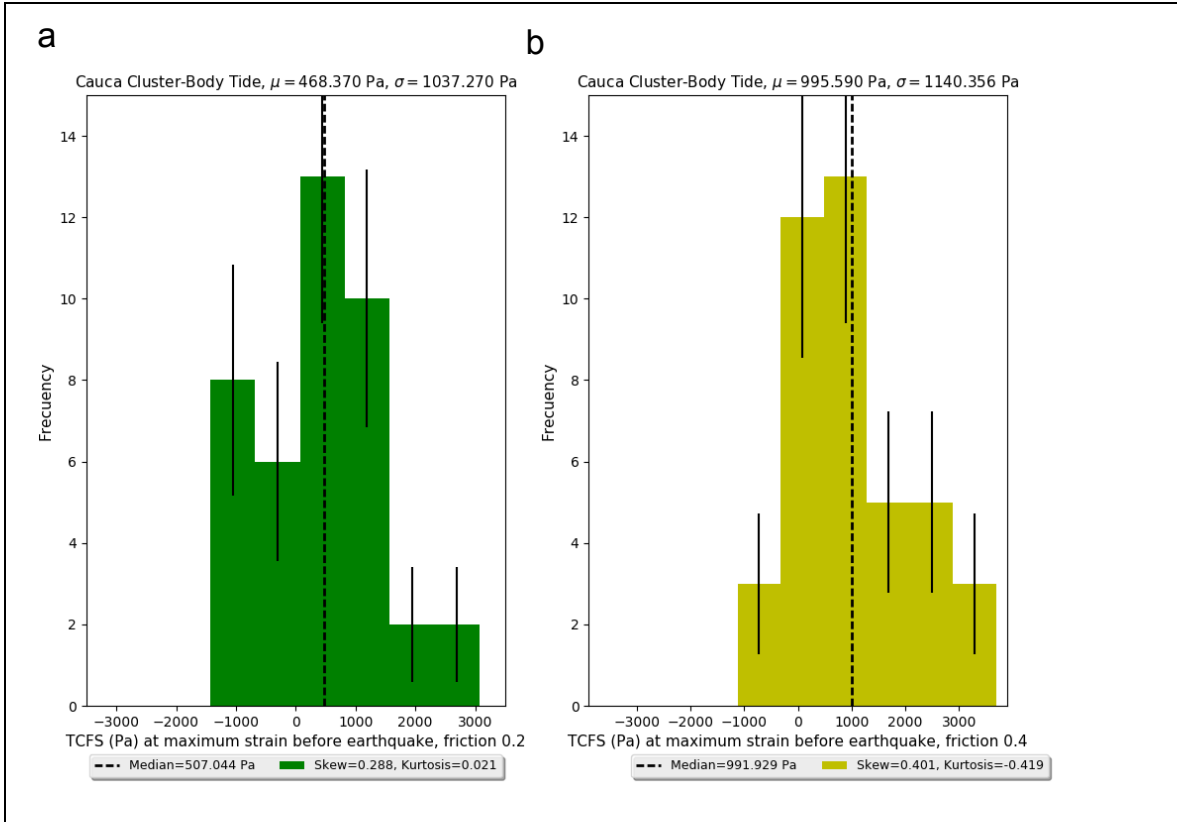


Figure 4. Frequency histograms of the TCFS for the Cauca seismic cluster, considering BT and OTL. Plot structure, conventions and assumptions are the same as in Figure 3.



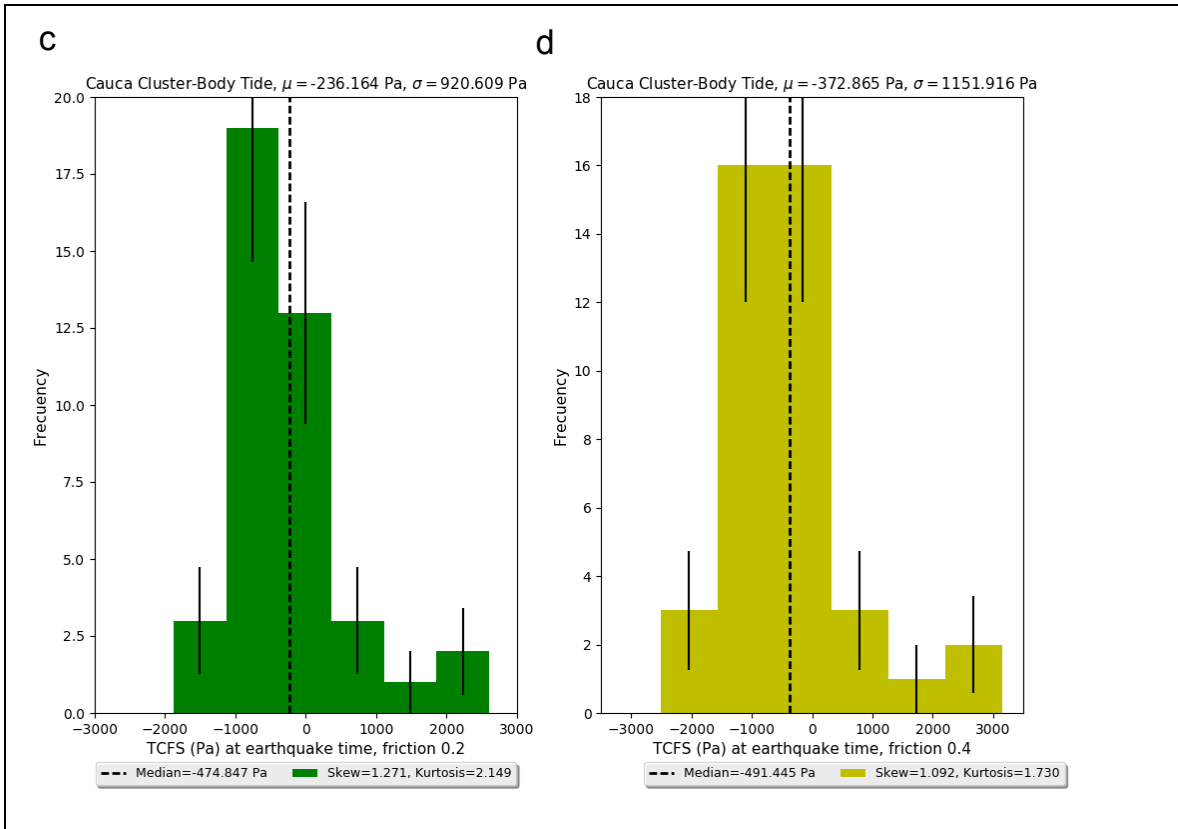


Figure 5. Frequency histograms of the TFCS for the Cauca seismic cluster, considering only BT. Plot structure, conventions and assumptions are the same as in Figure 3.

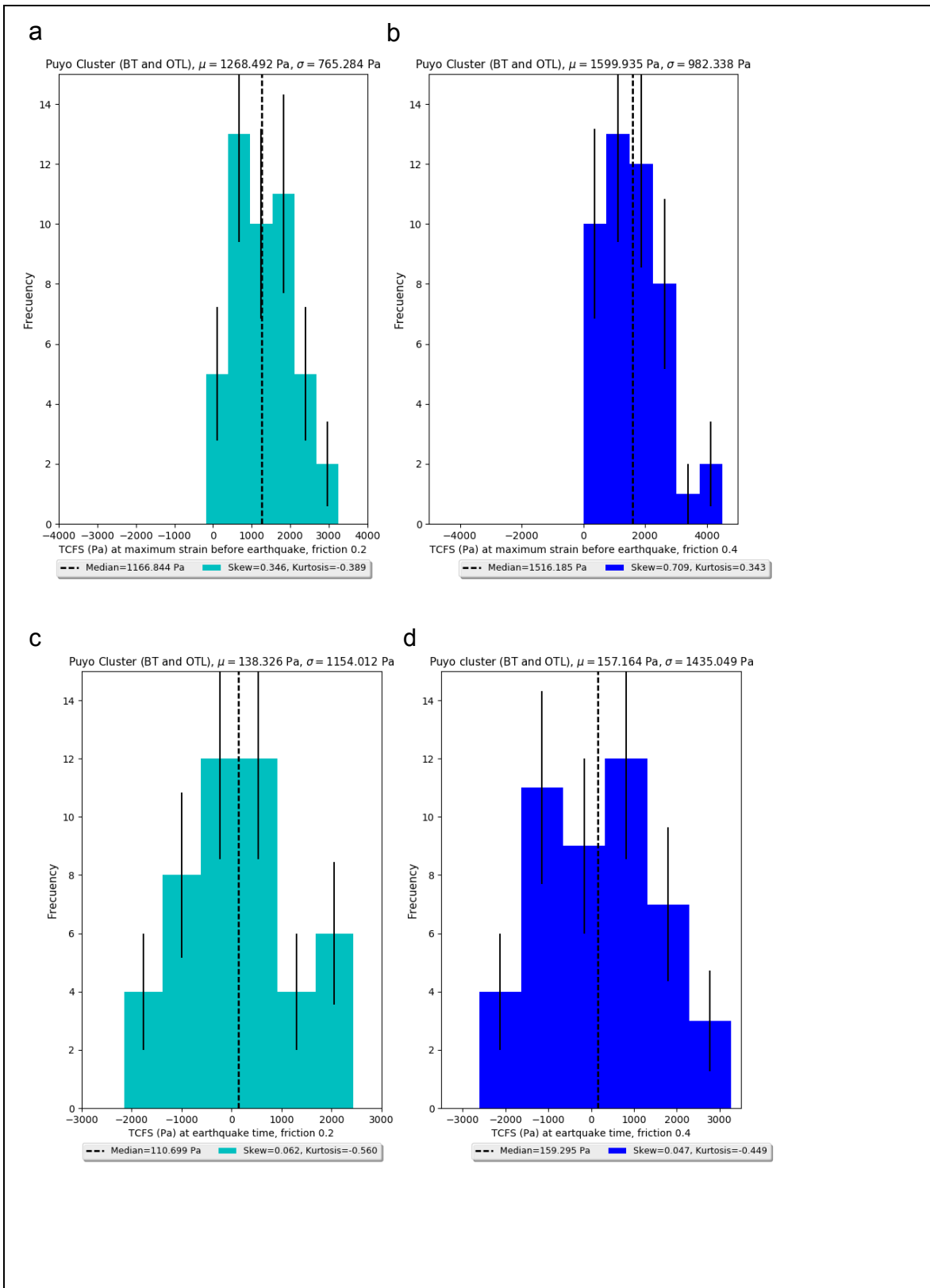


Figure 6. Frequency histograms of the TCFS for the Puyo (Ecuador) seismic cluster. Plot structure, conventions and assumptions are the same as in Figure 3.



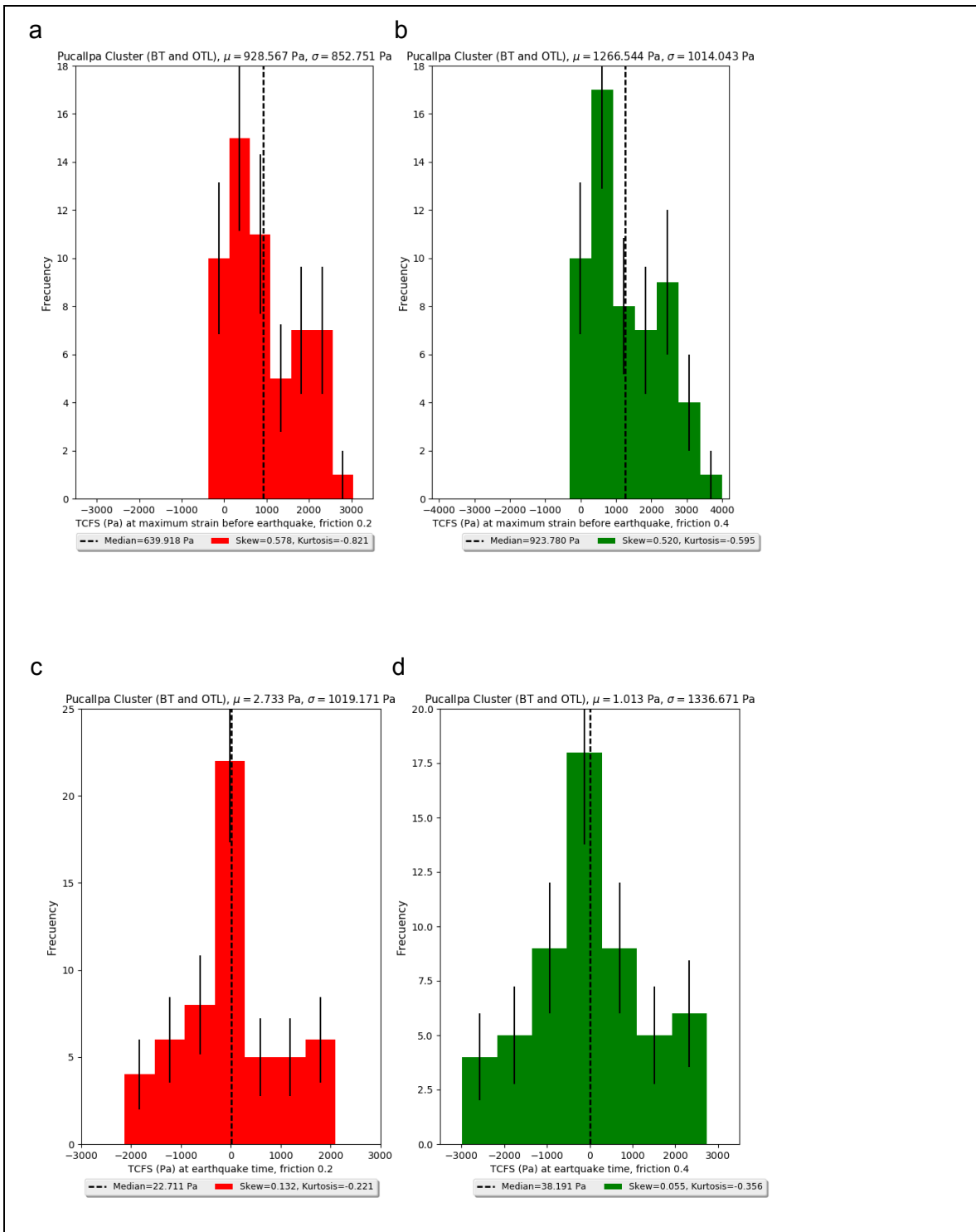


Figure 7. Frequency histograms of the TFCS for the Pucallpa (Peru) seismic cluster. Plot structure, conventions and assumptions are the same as in Figure 3.

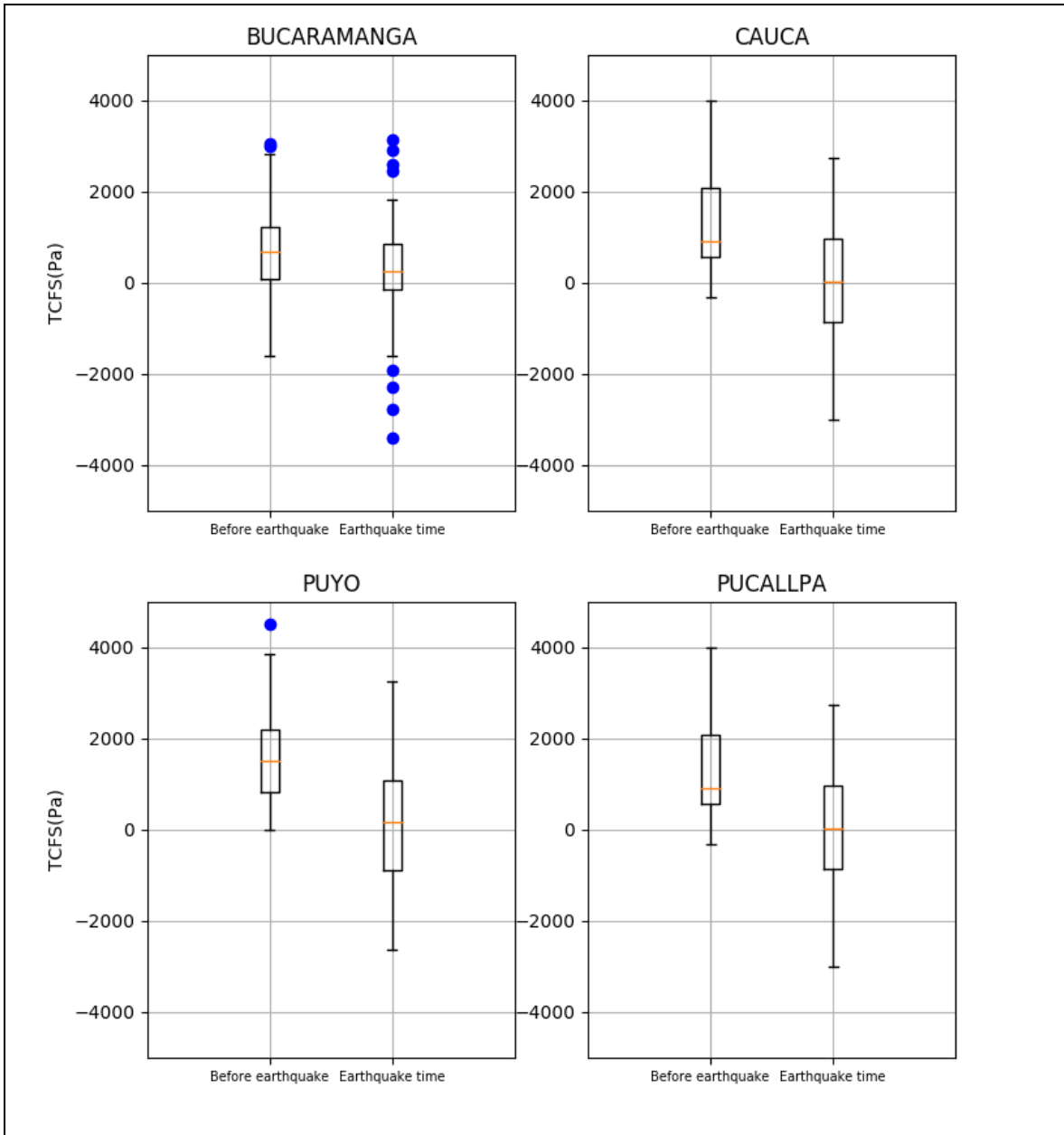


Figure 8. Box plots for the Bucaramanga, Cauca, Puyo and Pucallpa seismic clusters. Each panel includes information at the time of maximum strain before the earthquake (left) and during the earthquake time (right). The box plots correspond to the analysis made with a friction coefficient of 0.4. The orange lines show the median of the sample, which coincides with the second quartile. Inside each box we found the 50% of the sample. The blue circles represent atypical data, which are located at a greater distance than  $1.5 \cdot \text{IQR}$  ( $\text{IQR} = \text{interquartile range}$ ).

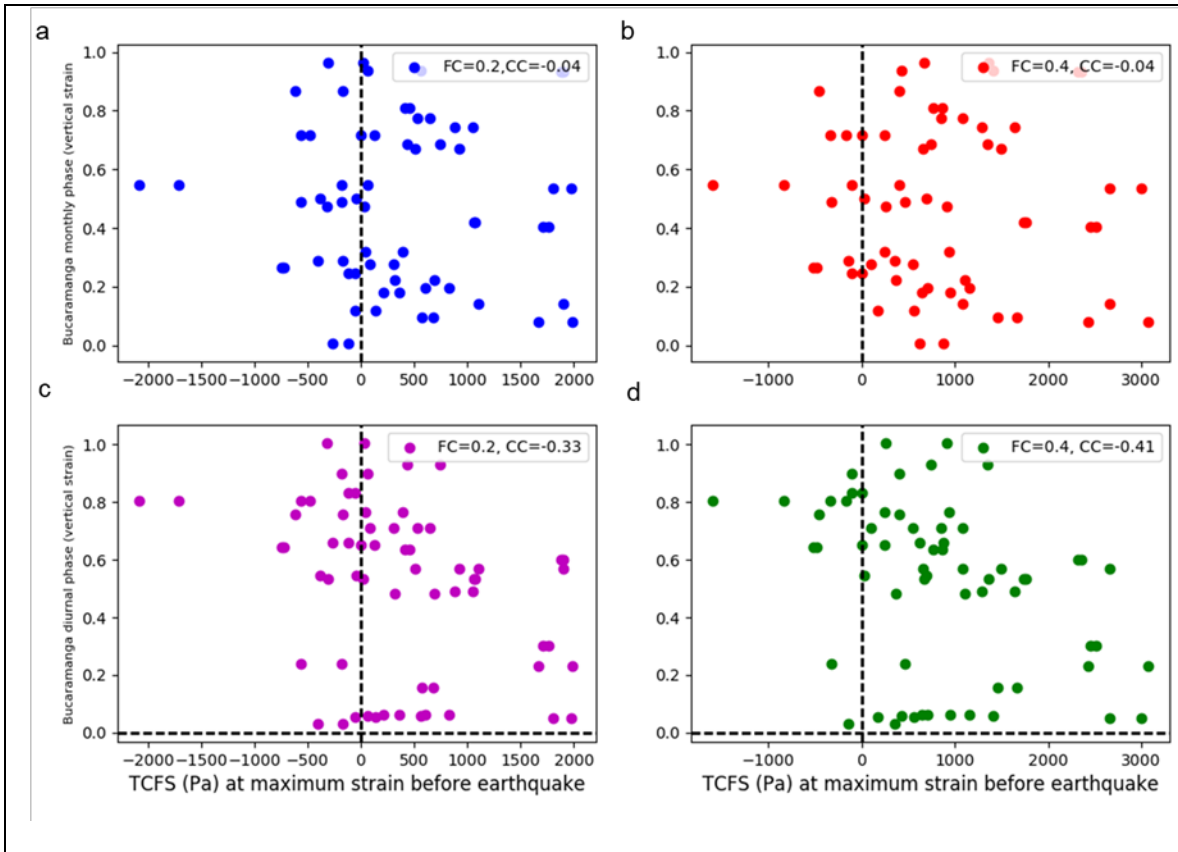


Figure 9. Scatter plots of the vertical strain vs the TCFS for the Bucaramanga seismic nest, using friction coefficients of 0.2 and 0.4 and a rigidity of 75 GPa. (a) and (b) consider the monthly phase, and (c) and (d) the diurnal phase. For the TCFS calculations we considered the time of maximum strain before the earthquake origin time. FC: Friction Coefficient; CC: Correlation Coefficient.

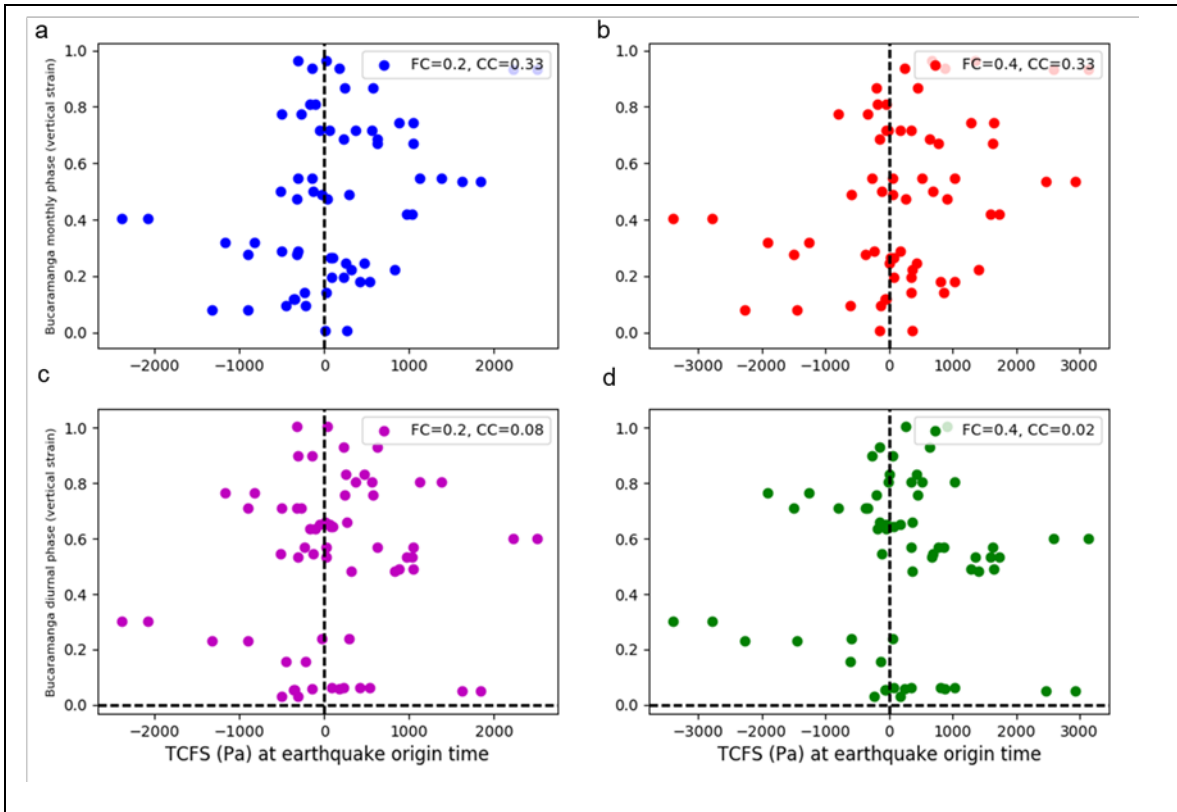


Figure 10. Same as in Figure 8, but using the strain at the earthquake origin time.

## Supplementary Material

Table S1. Calculated normal  $\sigma_N$  and shear  $\sigma_S$  tidal stress for 55 intermediate-depth events from 1977 to 2017 in the Bucaramanga seismic nest. At maximum strain before earthquake = MSBE and at earthquake origin time = AEOT. The data 1-39 combines information of Cortes and Angelier (2005) with information of the RSNC and CMT Catalog. NP1 corresponds to the strike (S), dip (D) and rake (R) of the first nodal plane. Date are in Julian Days.

No.	Julian Day	Lat °	Lon °	Depth (km)	MI	NP1			MSBE		AEOT	
						S	D	R	$\sigma_N$ (Pa)	$\sigma_S$ (Pa)	$\sigma_N$ (Pa)	$\sigma_S$ (Pa)
1	2443225.59097	7.17	-73.18	157.7	5.5	15	46	160	1941.62	-244.76	-1335.88	644.28
2	2443438.55764	7.58	-73.17	169.3	5.2	196	13	-52	158.902	495.22	158.90	495.23
3	2443888.30556	6.85	-73.21	157.4	5.1	261	8	-29	81.50	300.04	47.22	118.50
4	2443944.01111	7.03	-73.32	157.7	5.7	118	40	170	1799.32	-801.52	-1014.4	-87.20
5	2444467.39583	6.67	-73.12	166.0	5.1	257	15	-2	274.86	34.50	174.29	40.94
6	2445474.47361	7.11	-73.41	155.1	5.2	350	76	-14	2442.18	-123.42	2442.19	-123.42

No.	Julian Day	Lat °	Lon °	Depth (km)	MI	NP1			MSBE		AEOT	
						S	D	R	$\sigma_N$ (Pa)	$\sigma_S$ (Pa)	$\sigma_N$ (Pa)	$\sigma_S$ (Pa)
7	2445575.85000	6.64	-72.97	156.3	5.3	278	34	18	1334.27	-528.07	1360.85	-584.23
8	2446009.05139	7.28	-73.25	155.7	5.4	187	14	-96	179.56	717.93	133.05	548.56
9	2446243.48958	7.10	-73.00	144.2	5.1	12	9	76	77.52	-474.57	65.01	-434.44
10	2446403.24444	7.10	-73.34	153.4	5.3	34	59	179	1788.61	266.01	-444.65	523.08
11	2446611.34097	7.15	-73.14	160.1	5.7	259	46	18	1447.35	-702.65	93.82	252.46
12	2446734.79514	7.21	-73.13	153.2	5.2	131	33	-171	1948.58	-40.54	-125.56	315.31
13	2447693.16111	6.87	-73.09	156.8	5.2	109	8	-173	63.06	46.31	59.06	48.02
14	2448228.52639	6.78	-72.95	158.2	5.3	315	21	71	314.28	-647.30	-513.16	1198.62
15	2448987.56111	6.74	-72.96	154.3	5.1	41	42	124	738.75	-459.52	-592.05	284.62
16	2449697.14167	6.89	-72.85	164.4	5.2	45	42	121	1138.13	-968.06	-261.67	123.51
17	2449858.42986	5.66	-73.84	141.1	5.2	282	17	-7	251.98	269.66	266.74	259.69
18	2450449.69097	6.98	-72.91	164.3	5.3	126	48	146	1145.08	-789.72	-1050.9	765.94
19	2451490.74375	6.90	-73.15	160.2	5.4	54	38	152	2017.65	-782.86	2010.94	-920.45
20	2452233.37569	6.74	-72.90	153.7	5.3	324	73	-9	519.61	496.26	576.87	117.03
21	2453175.12500	6.82	-73.01	151.2	4.8	353	36	143	370.49	-257.23	154.76	-336.14
22	2453281.85417	6.83	-73.04	172.4	4.8	148	64	-170	2219.63	-235.51	1942.18	31.86
23	2453426.77847	6.88	-73.09	159.2	5.3	57	54	-176	4279.32	945.97	4232.95	771.32
24	2453745.63472	6.89	-73.20	171.6	5.0	32	43	151	1324.41	-668.72	1360.32	-771.71
25	2453864.12986	7.02	-73.24	168.4	4.9	71	66	180	3432.58	384.02	3100.64	346.59
26	2454257.69931	6.84	-73.13	156.6	5.4	36	49	173	1540.45	131.19	22.11	623.58
27	2454514.38542	6.82	-73.04	156.9	5.4	10	45	165	1023.81	-164.41	-2141.1	-391.11
28	2454941.87083	7.81	-73.53	129.6	5.1	300	28	40	781.49	-768.98	-622.13	693.35
29	2455132.18403	6.93	-73.07	164.2	5.1	42	54	175	1809.56	48.76	308.93	-170.78
30	2455982.07153	6.84	-73.02	150.5	5.1	226	42	52	2473.13	-2578.2	-1756.1	1735.60
31	2456171.71458	6.86	-73.12	164.4	5.1	48	43	151	2914.04	-901.88	2914.04	-901.88
32	2456487.00625	6.87	-73.13	155.1	5.0	72	67	-166	5369.29	918.69	-4778.31	-360.69
33	2456696.35903	6.81	-73.07	159.3	5.3	13	22	91	53.06	-126.41	-209.20	515.12
34	2456987.34722	6.89	-73.02	168.3	5.0	146	48	42	1177.06	-293.61	1474.02	-658.87

No.	Julian Day	Lat °	Lon °	Depth (km)	MI	NP1			MSBE		AEOT	
						S	D	R	$\sigma_N$ (Pa)	$\sigma_S$ (Pa)	$\sigma_N$ (Pa)	$\sigma_S$ (Pa)
35	2457005.57569	5.34	-73.69	158.5	4.8	250	9	-18	34.34	-3.65	-22.83	-42.45
36	2457092.37153	6.83	-73.11	155.9	6.2	142	29	-152	785.34	349.11	790.71	463.00
37	2457104.43542	6.98	-73.07	170.3	4.9	66	52	166	4433.09	-318.21	-813.01	-282.85
38	2457309.82431	7.73	-73.42	120.0	5.1	333	44	2	2115.98	293.22	1498.31	-33.20
39	2457653.94583	6.89	-73.10	157.8	4.8	51	58	19	2282.65	-979.32	2165.62	-426.16
40	2456739.36667	6.08	-73.14	152.0	4.4	77	89	-171	2947.06	459.05	2947.06	459.05
41	2456745.69097	6.83	-73.16	147.7	4.4	42	58	9	4922.54	-1294.1	4922.54	-1294.12
42	2456746.85833	6.79	-73.16	142.2	4.4	352	68	40	4472.18	-1163.5	473.92	171.19
43	2456888.75417	6.83	-73.16	154.4	4.2	152	23	-157	83.94	65.90	-222.14	-275.52
44	2456941.15069	6.82	-73.16	143.1	4.3	118	67	-153	2153.87	218.69	-1485.85	-196.55
45	2456981.73611	6.83	-73.17	157.0	4.3	355	54	-60	2179.06	1444.33	3159.78	1868.59
46	2457047.92708	6.82	-73.15	149.6	4.5	163	84	25	-90.77	1114.21	4170.03	-807.95
47	2457144.91042	6.81	-73.15	141.1	4.4	105	30	30	1204.45	-805.26	-1138.72	517.61
48	2457204.74653	6.80	-73.13	145.2	4.2	84	79	33	4190.14	-270.64	3473.38	-514.85
49	2457218.47639	6.79	-73.09	153.3	4.5	58	65	-156	3827.35	990.97	-3467.12	-1378.94
50	2457355.23958	6.82	-73.15	154.0	4.7	68	70	-157	4704.89	937.07	3048.23	606.01
51	2457425.00347	6.82	-73.12	153.0	4.2	50	48	20	2613.58	-1143.5	-557.43	117.13
52	2457429.80139	6.82	-73.14	154.2	4.5	177	74	42	4354.59	-1024.9	4890.39	-1067.06
53	2457446.72778	6.83	-73.13	150.0	4.2	105	65	44	3201.62	-755.78	524.29	313.30
54	2457456.76875	6.84	-73.15	148.3	4.7	130	36	58	2550.85	-2613.6	2352.93	-2538.26
55	2457508.99097	6.81	-73.16	145.5	4.2	329	75	-27	1682.38	503.43	1682.38	503.43

Table S2. Calculated normal  $\sigma_N$  and shear  $\sigma_S$  tidal stress for 55 intermediate-depth events from 1977 to 2017 in the Bucaramanga seismic nest. At maximum strain before earthquake = MSBE and at earthquake origin time = AEOT. The data 1-39 combines information of Cortes and Angelier (2005) with information of the RSN and CMT Catalog. NP2 corresponds to the strike (S), dip (D) and rake (R) of the second nodal plane. Date in days of the Julian Calendar (JC) since the reference time 4713 B.C.

No.	Date (days in JC)	Lat °	Lon °	Depth (km)	MI	NP2			MSBE		AEOT	
						S	D	R	$\sigma_N$ (Pa)	$\sigma_S$ (Pa)	$\sigma_N$ (Pa)	$\sigma_S$ (Pa)
1	2443225.59097	7.17	-73.18	157.7	5.5	119	76	46	4468.00	-239.00	-3287.52	639.13
2	2443438.55764	7.58	-73.17	169.3	5.2	337	80	-98	3083.84	485.12	3083.84	485.12
3	2443888.30556	6.85	-73.21	157.4	5.1	20	86	-97	2690.50	306.97	1885.99	123.14
4	2443944.01111	7.03	-73.32	157.7	5.7	216	83	51	4066.37	-831.44	-1475.32	-68.35
5	2444467.39583	6.67	-73.12	166.0	5.1	349	89	-105	2310.11	53.85	2136.42	58.47
6	2445474.47361	7.11	-73.41	155.1	5.2	83	76	-166	3274.31	-116.84	3274.31	-116.84
7	2445575.85000	6.64	-72.97	156.3	5.3	173	80	123	2598.49	-528.53	3040.18	-584.97
8	2446009.05139	7.28	-73.25	155.7	5.4	14	76	-88	2919.96	720.63	2316.55	549.50
9	2446243.48958	7.10	-73.00	144.2	5.1	206	81	92	3154.04	-489.90	3072.49	-451.12
10	2446403.24444	7.10	-73.34	153.4	5.3	124	89	31	2406.36	263.14	-1967.75	536.11
11	2446611.34097	7.15	-73.14	160.1	5.7	156	77	135	2413.34	-707.22	-970.58	249.44
12	2446734.79514	7.21	-73.13	153.2	5.2	33	85	-58	6162.86	-16.54	-537.11	308.01
13	2447693.16111	6.87	-73.09	156.8	5.2	12	89	-82	2677.92	47.71	2912.58	49.44
14	2448228.52639	6.78	-72.95	158.2	5.3	155	70	97	1706.22	-653.91	-3494.94	1210.29
15	2448987.56111	6.74	-72.96	154.3	5.1	178	56	63	861.52	-455.82	-172.42	274.04
16	2449697.14167	6.89	-72.85	164.4	5.2	186	55	65	1208.73	-967.74	-134.96	123.35
17	2449858.42986	5.66	-73.84	141.1	5.2	20	88	-106	2105.46	263.82	2881.47	251.42
18	2450449.69097	6.98	-72.91	164.3	5.3	240	66	47	1528.67	-780.39	-1902.34	754.47
19	2451490.74375	6.90	-73.15	160.2	5.4	167	73	55	3715.47	-790.52	4023.97	-928.02
20	2452233.37569	6.74	-72.90	153.7	5.3	56	82	-162	1636.90	504.93	-80.76	109.13
21	2453175.12500	6.82	-73.01	151.2	4.8	114	69	60	1689.21	-269.35	997.33	-343.02
22	2453281.85417	6.83	-73.04	172.4	4.8	54	81	-27	2933.63	-226.09	2468.46	37.86
23	2453426.77847	6.88	-73.09	159.2	5.3	325	87	-36	5190.51	927.38	5434.40	753.51
24	2453745.63472	6.89	-73.20	171.6	5.0	144	70	51	2613.65	-692.76	2422.55	-792.46
25	2453864.12986	7.02	-73.24	168.4	4.9	161	90	24	3401.41	384.03	3481.30	346.59
26	2454257.69931	6.84	-73.13	156.6	5.4	131	85	41	3011.21	144.32	-1897.87	608.82
27	2454514.38542	6.82	-73.04	156.9	5.4	111	80	46	2702.70	-143.79	-3714.64	-415.51
28	2454941.87083	7.81	-73.53	129.6	5.1	173	73	112	2882.40	-748.32	-2182.61	677.90

No.	Date (days in JC)	Lat °	Lon °	Depth (km)	MI	NP2			MSBE		AEOT	
						S	D	R	$\sigma_N$ (Pa)	$\sigma_S$ (Pa)	$\sigma_N$ (Pa)	$\sigma_S$ (Pa)
29	2455132.18403	6.93	-73.07	164.2	5.1	135	86	36	2046.88	49.50	-10.13	-171.41
30	2455982.07153	6.84	-73.02	150.5	5.1	93	58	119	4407.77	-2589.9	-3071.30	1743.29
31	2456171.71458	6.86	-73.12	164.4	5.1	159	71	50	4422.84	-849.37	4422.84	-849.37
32	2456487.00625	6.87	-73.13	155.1	5.0	337	77	-24	3822.74	904.96	-2746.70	-342.23
33	2456696.35903	6.81	-73.07	159.3	5.3	191	68	90	280.23	-113.22	-1256.90	507.82
34	2456987.34722	6.89	-73.02	168.3	5.0	25	60	130	2110.44	-286.22	1539.62	-656.02
35	2457005.57569	5.34	-73.69	158.5	4.8	357	87	-98	615.34	-0.66	510.79	-32.94
36	2457092.37153	6.83	-73.11	155.9	6.2	26	77	-64	2881.08	346.37	2936.39	459.57
37	2457104.43542	6.98	-73.07	170.3	4.9	164	79	39	4895.31	-301.06	425.40	-299.86
38	2457309.82431	7.73	-73.42	120.0	5.1	242	88	134	5753.03	241.84	3068.70	-56.53
39	2457653.94583	6.89	-73.10	157.8	4.8	310	74	147	2943.04	-975.62	2682.17	-421.40
40	2456739.36667	6.08	-73.14	152.0	4.4	346	81	-1	2057.13	471.15	2057.13	471.15
41	2456745.69097	6.83	-73.16	147.7	4.4	308	82	148	6676.61	-1314.4	6676.61	-1314.43
42	2456746.85833	6.79	-73.16	142.2	4.4	245	54	153	4993.02	-1114.3	-816.76	171.55
43	2456888.75417	6.83	-73.16	154.4	4.2	41	81	-69	1192.95	73.76	-2988.73	-293.26
44	2456941.15069	6.82	-73.16	143.1	4.3	17	65	-25	1594.56	213.47	-366.66	-191.04
45	2456981.73611	6.83	-73.17	157.0	4.3	130	46	-125	2325.52	1433.68	1839.68	1858.32
46	2457047.92708	6.82	-73.15	149.6	4.5	70	65	174	3785.24	1147.69	2844.60	-796.94
47	2457144.91042	6.81	-73.15	141.1	4.4	348	75	117	3247.36	-833.25	-2844.57	541.13
48	2457204.74653	6.80	-73.13	145.2	4.2	346	58	167	1807.71	-293.60	1939.28	-525.73
49	2457218.47639	6.79	-73.09	153.3	4.5	318	69	-27	3713.35	971.96	-5038.24	-1373.99
50	2457355.23958	6.82	-73.15	154.0	4.7	330	69	-22	3675.03	931.85	683.41	595.46
51	2457425.00347	6.82	-73.12	153.0	4.2	306	75	136	4391.04	-1158.8	-2816.83	121.89
52	2457429.80139	6.82	-73.14	154.2	4.5	73	50	159	4258.36	-1016.5	4191.85	-1059.38
53	2457446.72778	6.83	-73.13	150.0	4.2	353	51	147	1482.42	-752.63	-162.39	315.74
54	2457456.76875	6.84	-73.15	148.3	4.7	347	60	111	4709.03	-2630.6	4573.92	-2551.11
55	2457508.99097	6.81	-73.16	145.5	4.2	67	64	-163	1773.17	503.91	1773.17	503.91



Table S3. Focal mechanism information for 22 intermediate-depth events from 1977 to 2017 in the Cauca seismic cluster. At maximum strain before earthquake = MSBE and at earthquake origin time = AEOT. The data combines information of Cortes and Angelier (2005) (C&A2005) with information from the RSNL, CMT Catalog, Salcedo et al., 2001, and Tabares et al., 1999. NP1 corresponds to the strike (S), dip (D) and rake (R) of the first nodal plane. Date in days of the Julian Calendar (JC) since the reference time 4713 B.C.

No.	Date (days in JC)	Lat °	Lon °	Depth (km)	MI	NP1			MSBE		AEOT	
						S	D	R	$\sigma_N$ (Pa)	$\sigma_S$ (Pa)	$\sigma_N$ (Pa)	$\sigma_S$ (Pa)
1	2444416.00347	4,70	-75,35	151,0	6,3	231	74	14	2625,79	-1086,8	-1485,82	-728,20
2	2448219.44097	4,45	-75,46	147,0	6,0	182	23	-139	11,46	45,03	215,27	243,24
3	2450337.76944	4,59	-76,90	118,2	5,3	306	51	144	2124,31	-2458,1	1867,60	-70,48
4	2450499.26736	4,78	-76,50	118,1	5,8	138	42	105	926,05	-1259,9	1146,83	-1033,93
5	2450794.05972	4,11	-75,84	189,5	6,3	249	53	31	3171,06	-1740,4	1883,25	-1416,30
6	2452174.64097	4,03	-76,17	178,0	5,9	247	53	31	2786,31	-2331,4	-1852,57	280,79
7	2454722.89722	4,94	-75,48	139,8	5,7	227	13	-115	245,60	1088,17	-224,26	-984,77
8	2455184.10417	3,08	-76,30	169,2	5,1	110	46	-172	2055,78	102,02	-1580,39	-674,81
9	2455226.24444	4,83	-76,07	128,0	4,9	195	41	-72	1404,72	1253,66	2067,21	2155,16
10	2457075.43472	4,80	-76,06	102,7	5,2	93	51	-179	4566,74	-280,00	-302,92	426,98
11	2457076.03889	2,73	-76,46	161,3	5,6	119	45	-156	3247,70	555,61	-1913,32	-105,82
12	2439129.26111	4,65	-76,00	98,0	5,1	351	78	-157	1643,44	223,85	397,08	-349,56
13	2441776.07917	4,70	-75,80	158,0	6,1	21	72	-32	3956,15	-689,23	-2939,73	-980,56
14	2441797.27917	5,20	-75,80	117,0	5,3	23	82	21	-567,06	-1026,6	-1992,79	-48,85
15	2442515.57847	4,85	-75,71	139,0	5,1	232	53	163	3272,67	415,89	-1999,50	436,32
16	2442918.20417	4,50	-75,80	166,0	5,8	40	74	-130	580,23	1170,93	-2628,75	-851,28
17	2446518.90833	4,59	-75,63	163,0	5,0	230	74	154	4121,19	1519,05	2375,46	-879,56
18	2447527.37361	5,10	-75,78	118,0	4,9	46	48	27	1074,95	-999,86	-563,08	-482,57
19	2448624.32014	5,67	-73,84	146,0	5,7	170	55	180	582,38	160,57	-596,94	-576,77
20	2444023.04097	5,28	-75,73	122,0	4,9	174	44	-100	-286,99	-279,25	-566,97	-664,63
21	2444201.48611	4,81	-76,20	105,0	6,3	210	90	-150	207,92	2157,26	-155,73	-2182,30
22	2448850.29306	5,15	-75,58	107,0	5,6	288	22	-71	737,10	1892,01	673,00	1627,77

Table S4. Focal mechanism information for 22 intermediate-depth events from 1977 to 2017 in the Cauca seismic cluster. At maximum strain before earthquake = MSBE and at earthquake origin time = AEOT. The data combines information of Cortes and Angelier (2005) (C&A2005) with information from the RSNL, CMT Catalog, Salcedo et al., 2001, and Tabares et al., 1999. NP2 corresponds to

the strike (S), dip (D) and rake (R) of the second nodal plane. Date in days of the Julian Calendar since the reference time 4713 B.C.

No.	Date (days in JC)	Lat °	Lon °	Depth (km)	MI	NP2			MSBE		AEOT	
						S	D	R	$\sigma_N$ (Pa)	$\sigma_S$ (Pa)	$\sigma_N$ (Pa)	$\sigma_S$ (Pa)
1	2444416.00347	4,70	-75,35	151,0	6,3	137	76	164	1488,05	-1089,2	-575.61	-726.71
2	2448219.44097	4,45	-75,46	147,0	6,0	53	75	-72	1346,39	40,10	1019.79	245.94
3	2450337.76944	4,59	-76,90	118,2	5,3	61	63	45	3612,54	-2448,0	1913.32	-69.61
4	2450499.26736	4,78	-76,50	118,1	5,8	299	50	77	1834,25	-1235,6	1023.58	-1050.44
5	2450794.05972	4,11	-75,84	189,5	6,3	140	66	139	3712,29	-1722,0	231.76	-1393.03
6	2452174.64097	4,03	-76,17	178,0	5,9	137	65	139	2049,77	-2342,3	-1359.31	289.11
7	2454722.89722	4,94	-75,48	139,8	5,7	72	79	-85	5522,24	1019,97	-4801.62	-922.60
8	2455184.10417	3,08	-76,30	169,2	5,1	14	84	-44	770,47	121,39	-4223.22	-681.33
9	2455226.24444	4,83	-76,07	128,0	4,9	352	51	-105	1613,05	1261,67	2792.11	2163.50
10	2457075.43472	4,80	-76,06	102,7	5,2	2	89	-39	2029,11	-247,23	5042.58	411.43
11	2457076.03889	2,73	-76,46	161,3	5,6	12	74	-48	2918,08	516,04	1081.54	-82.68
12	2439129.26111	4,65	-76,00	98,0	5,1	256	67	-13	3078,41	230,66	-2030.32	-354.34
13	2441776.07917	4,70	-75,80	158,0	6,1	122	60	-160	4907,91	-756,86	-904.40	-980.61
14	2441797.27917	5,20	-75,80	117,0	5,3	110	68	172	549,63	-1020,2	-312.07	-50.33
15	2442515.57847	4,85	-75,71	139,0	5,1	325	85	-143	4069,84	-927,11	-4442.06	-173.58
16	2442918.20417	4,50	-75,80	166,0	5,8	156	44	-30	-116,79	700,24	-751.73	-278.20
17	2446518.90833	4,59	-75,63	163,0	5,0	327	65	18	1812,49	1532,64	2862.22	-895.32
18	2447527.37361	5,10	-75,78	118,0	4,9	298	71	135	1175,57	-989,31	262.19	-498.30
19	2448624.32014	5,67	-73,84	146,0	5,7	260	90	35	2543,81	160,57	-3045.86	-576.77

Table S5. Focal mechanism information for intermediate-depth events from 1986 to 2016 in the region of the Puyo seismic cluster. At maximum strain before earthquake = MSBE and at earthquake origin time = AEOT. The information about focal mechanism was obtained from CMT Catalog. Conventions as in Tables S1.

No.	Date (days in JC)	Lat °	Lon °	Depth (km)	MI	NP1			MSBE		AEOT	
						S	D	R	$\sigma_N$ (Pa)	$\sigma_S$ (Pa)	$\sigma_N$ (Pa)	$\sigma_S$ (Pa)
1	2445110,01	-1,41	-78,25	181,1	5,3	176	19	-36	-60.86	21.18	-60,86	21,18
2	2446451,79	-1,84	-77,76	166,3	5,4	157	25	-51	123.76	168.36	-314,19	-773,12

No.	Date (days in JC)	Lat °	Lon °	Depth (km)	MI	NP1			MSBE		AEOT	
						S	D	R	$\sigma_N$ (Pa)	$\sigma_S$ (Pa)	$\sigma_N$ (Pa)	$\sigma_S$ (Pa)
3	2447147,71	-1,26	-77,90	172,9	5,5	142	25	-76	599.02	1296.94	235,90	470,03
4	2447420,28	-1,25	-78,01	169,0	6,2	121	28	-109	956.67	1640.46	700,85	1169,34
5	2449377,74	-1,72	-77,79	154,3	5,4	195	35	-36	1045.53	657.35	1011,38	516,82
6	2450110,52	-1,79	-77,71	149,0	5,3	149	24	-63	223.72	509.12	194,70	396,95
7	2451295,26	-1,50	-77,83	164,2	6,0	169	33	-49	1096.50	1350.41	358,26	265,93
8	2451419,03	-1,36	-77,75	198,2	6,2	122	18	-107	616.56	1735.99	-416,50	-1141,67
9	2453542,92	-1,86	-78,02	166,1	5,0	131	16	-94	275.76	949.10	-325,04	-1108,73
10	2453728,41	-1,59	-77,76	196,8	6,1	120	21	-107	221.92	498.15	218,46	552,42
11	2453908,03	-2,06	-77,42	165,8	5,3	185	36	-29	1222.40	561.95	202,74	553,61
12	2454039,91	-1,53	-78,04	177,5	5,4	137	29	-80	871.11	1578.57	-132,06	-217,44
13	2454106,77	-1,52	-78,09	164,4	5,0	127	40	-102	1569.22	1755.19	1481,49	1648,05
14	2454145,12	-1,60	-78,05	175,8	5,6	139	25	-95	185.28	390.83	288,34	609,67
15	2454155,09	-1,58	-78,08	160,1	5,0	95	52	-154	2904.72	696.94	-1521,10	-265,98
16	2454188,37	-1,60	-77,81	191,5	5,3	104	24	-124	395.65	710.96	-411,83	-509,63
17	2454303,29	-1,66	-78,30	158,7	5,2	132	23	-101	310.77	694.17	-200,04	-467,17
18	2454651,75	-1,58	-77,91	193,4	5,2	122	32	-119	1100.08	1358.64	1343,91	1740,72
19	2454952,52	-1,74	-77,66	194,9	5,1	153	21	-62	204.19	480.87	73,39	45,43
20	2455421,00	-1,51	-77,51	197,8	7,1	153	21	-68	783.52	2028.74	-225,88	-651,40
21	2456070,93	-1,96	-78,00	158,8	4,8	125	15	-102	203.46	720.93	-112,74	-368,92
22	2456973,08	-2,00	-78,23	163,2	4,8	135	37	-110	795.16	877.95	-1457,07	-1707,94
23	2457662,20	-1,80	-77,75	185,0	5,0	159	24	-71	733.06	1650.56	694,20	1581,66

Table S6. Focal mechanism information for intermediate-depth events from 1986 to 2016 in the region of the Puyo seismic cluster. At maximum strain before earthquake = MSBE and at earthquake origin time = AEOT. The information about focal mechanism was obtained from CMT Catalog. Conventions as in Table S2.

No.	Date (days in JC)	Lat °	Lon °	Depth (km)	MI	NP2			MSBE		AEOT	
						S	D	R	$\sigma_N$ (Pa)	$\sigma_S$ (Pa)	$\sigma_N$ (Pa)	$\sigma_S$ (Pa)
1	2445110,01	-1,41	-78,25	181,1	5,3	300	79	-105	253.87	24.76	253,87	24,76

No.	Date (days in JC)	Lat °	Lon °	Depth (km)	MI	NP2			MSBE		AEOT	
						S	D	R	$\sigma_N$ (Pa)	$\sigma_S$ (Pa)	$\sigma_N$ (Pa)	$\sigma_S$ (Pa)
2	2446451,79	-1,84	-77,76	166,3	5,4	295	71	-107	919.39	160.35	-1833,44	-773,49
3	2447147,71	-1,26	-77,90	172,9	5,5	306	66	-97	3037.23	1286.34	1135,93	463,64
4	2447420,28	-1,25	-78,01	169,0	6,2	322	64	-80	3164.24	1630.04	2197,76	1163,79
5	2449377,74	-1,72	-77,79	154,3	5,4	316	70	-120	2826.64	661.39	2011,81	522,49
6	2450110,52	-1,79	-77,71	149,0	5,3	300	68	-102	1326.49	522.00	1077,23	406,86
7	2451295,26	-1,50	-77,83	164,2	6,0	304	66	-113	3732.28	1328.80	627,11	269,63
8	2451419,03	-1,36	-77,75	198,2	6,2	320	73	-85	5348.81	1712.44	-3457,51	-1124,41
9	2453542,92	-1,86	-78,02	166,1	5,0	316	74	-89	3270.08	945.98	-3787,76	-1101,04
10	2453728,41	-1,59	-77,76	196,8	6,1	318	69	-84	1297.29	516.24	1395,48	570,37
11	2453908,03	-2,06	-77,42	165,8	5,3	299	74	-122	3473.52	543.13	2072,21	542,89
12	2454039,91	-1,53	-78,04	177,5	5,4	306	61	-95	2942.22	1597.78	-410,61	-221,02
13	2454106,77	-1,52	-78,09	164,4	5,0	322	51	-80	2103.99	1761.38	1935,39	1655,66
14	2454145,12	-1,60	-78,05	175,8	5,6	325	65	-88	833.66	390.97	1301,31	610,07
15	2454155,09	-1,58	-78,08	160,1	5,0	348	70	41	3164.48	-816.71	-1319,79	363,42
16	2454188,37	-1,60	-77,81	191,5	5,3	321	70	-76	1944.24	718.13	-1406,99	-510,10
17	2454303,29	-1,66	-78,30	158,7	5,2	325	68	-85	1544.69	678.72	-1145,47	-458,22
18	2454651,75	-1,58	-77,91	193,4	5,2	335	62	-73	2640.26	1371.49	3275,46	1756,74
19	2454952,52	-1,74	-77,66	194,9	5,1	304	71	-100	1663.82	494.80	351,72	51,59
20	2455421,00	-1,51	-77,51	197,8	7,1	309	71	-98	6275.20	2001.81	-2143,31	-645,79
21	2456070,93	-1,96	-78,00	158,8	4,8	317	76	-87	2683.84	692.25	-1284,87	-355,71
22	2456973,08	-2,00	-78,23	163,2	4,8	340	56	-76	1125.20	865.85	-2276,92	-1689,40
23	2457662,20	-1,80	-77,75	185,0	5,0	318	67	-98	4283.23	1682.96	4137,88	1613,89

Table S7. Focal mechanism information for intermediate-depth events from 1986 to 2016 in the region of the Pucallpa seismic cluster. At maximum strain before earthquake = MSBE and at earthquake origin time = AEOT. The information about focal mechanism was obtained from CMT Catalog. Conventions as in Table S1.

No.	Date (days in JC)	Lat °	Lon °	Depth (km)	MI	NP1			MSBE		AEOT	
						S	D	R	$\sigma_N$ (Pa)	$\sigma_S$ (Pa)	$\sigma_N$ (Pa)	$\sigma_S$ (Pa)
1	2443216,39	-7,95	-74,52	153,0	-7,95	62	17	149	263.53	-421.51	-190,77	459,43
2	2444333,77	-7,44	-74,49	164,7	-7,44	196	59	-17	2156.11	197.78	2630,53	170,36
3	2445304,42	-8,52	-73,50	149,7	-8,52	291	52	6	4150.95	136.16	-3370,88	-886,16
4	2446529,25	-7,76	-73,82	179,0	-7,76	206	27	-66	978.84	1623.26	894,79	1479,36
5	2447545,23	-7,34	-74,25	148,1	-7,34	10	47	-117	1733.80	1499.39	957,87	663,85
6	2447864,09	-7,37	-74,27	150,9	-7,37	192	40	-70	592.49	588.70	-743,64	-993,38
7	2448586,09	-8,47	-74,48	146,6	-8,47	211	11	-41	79.09	166.49	-84,25	-284,07
8	2449728,94	-7,94	-74,21	177,0	-7,94	157	39	-164	242.87	-141.28	-577,72	109,31
9	2450198,21	-7,89	-74,03	160,6	-7,89	222	55	-39	1031.87	409.31	-1635,64	-589,45
10	2450883,24	-8,11	-73,89	161,9	-8,11	221	27	-65	994.19	1651.23	846,32	1426,52
11	2450907,42	-7,96	-74,48	153,7	-7,96	68	13	166	115.94	-107.26	38,19	38,31
12	2451849,69	-7,99	-74,35	153,1	-7,99	75	10	-179	90.19	18.82	-61,92	141,94
13	2452123,11	-7,16	-74,01	195,4	-7,16	20	43	-53	1455.13	1137.88	64,58	100,52
14	2452272,42	-8,15	-74,23	161,5	-8,15	303	4	50	23.30	-237.27	-22,37	186,22
15	2453151,66	-8,37	-74,37	164,1	-8,37	32	8	128	16.58	-54.78	-14,88	92,92
16	2453893,60	-7,58	-73,89	197,2	-7,58	234	45	-61	1853.18	1520.03	1981,38	1639,71
17	2454293,72	-8,00	-74,42	156,4	-8,00	215	37	-29	668.32	70.66	604,16	53,99
18	2454705,39	-7,76	-74,49	158,2	-7,76	198	39	-60	537.71	406.00	-858,77	-1055,62
19	2455222,45	-8,53	-74,52	148,3	-8,53	83	33	-130	837.22	876.15	-790,32	-503,80
20	2455464,29	-7,90	-74,53	155,8	-7,90	207	27	-38	1039.79	1003.66	731,05	754,71
21	2455717,07	-7,84	-74,46	154,2	-7,84	163	43	-100	1775.68	1863.11	-1553,53	-1722,61
22	2455798,24	-7,68	-74,66	144,4	-7,68	197	40	-57	498.96	359.63	-158,52	-385,00
23	2456141,90	-8,58	-74,36	150,5	-8,58	222	26	-66	1202.99	2122.19	-441,10	-693,91
24	2457158,56	-7,81	-74,42	160,7	-7,81	8	42	-72	1800.72	1850.99	870,58	856,21
25	2457418,82	-8,25	-74,29	160,7	-8,25	82	15	179	128.21	104.53	34,45	-26,09
26	2457448,87	-7,85	-74,38	155,6	-7,85	208	38	-46	687.19	534.99	-284,76	-143,16
27	2457704,12	-8,44	-74,53	148,4	-8,44	140	48	-170	2676.74	-193.48	2848,52	-161,82
28	2457877,60	-8,56	-74,42	156,1	-8,56	73	22	-167	372.04	186.13	331,67	2,59

Table S8. Focal mechanism information for intermediate-depth events from 1986 to 2016 in the region of the Pucallpa seismic cluster. At maximum strain before earthquake = MSBE and at earthquake origin time = AEOT. The information about focal mechanism was obtained from CMT Catalog. Conventions as in Table S2.

No.	Date (days in JC)	Lat °	Lon °	Depth (km)	MI	NP2			MSBE		AEOT	
						S	D	R	$\sigma_N$ (Pa)	$\sigma_S$ (Pa)	$\sigma_N$ (Pa)	$\sigma_S$ (Pa)
1	2443216,39	-7,95	-74,52	153,0	-7,95	182	81	75	2557.57	-436.46	-1527,20	472,79
2	2444333,77	-7,44	-74,49	164,7	-7,44	295	76	148	4122.26	-914.53	4143,17	-947,22
3	2445304,42	-8,52	-73,50	149,7	-8,52	198	85	142	5764.65	129.41	-5288,77	-874,45
4	2446529,25	-7,76	-73,82	179,0	-7,76	359	66	-101	3731.15	1601.58	3217,23	1454,54
5	2447545,23	-7,34	-74,25	148,1	-7,34	227	50	-64	2046.72	1493.31	814,55	660,27
6	2447864,09	-7,37	-74,27	150,9	-7,37	347	53	-106	848.72	588.65	-1681,97	-983,91
7	2448586,09	-8,47	-74,48	146,6	-8,47	341	83	-98	1891.37	162.88	-3620,44	-282,18
8	2449728,94	-7,94	-74,21	177,0	-7,94	54	80	-52	520.07	-141.41	-824,17	106,89
9	2450198,21	-7,89	-74,03	160,6	-7,89	338	59	-138	1173.96	407.94	-894,64	-607,33
10	2450883,24	-8,11	-73,89	161,9	-8,11	13	66	-102	3604.90	1634.04	3134,23	1412,16
11	2450907,42	-7,96	-74,48	153,7	-7,96	172	87	77	1996.41	-103.50	340,83	40,08
12	2451849,69	-7,99	-74,35	153,1	-7,99	345	90	-80	2569.72	9.89	-1116,86	148,09
13	2452123,11	-7,16	-74,01	195,4	-7,16	155	57	-119	2086.10	1143.66	668,64	94,50
14	2452272,42	-8,15	-74,23	161,5	-8,15	163	87	92	4343.00	-231.49	-4009,70	188,22
15	2453151,66	-8,37	-74,37	164,1	-8,37	173	84	85	240.18	-52.16	-1622,49	86,12
16	2453893,60	-7,58	-73,89	197,2	-7,58	15	52	-116	1890.88	1508.32	2081,12	1628,21
17	2454293,72	-8,00	-74,42	156,4	-8,00	329	73	-124	1163.45	66.28	225,29	55,56
18	2454705,39	-7,76	-74,49	158,2	-7,76	341	57	-112	738.13	404.18	-2310,75	-1062,69
19	2455222,45	-8,53	-74,52	148,3	-8,53	308	65	-67	1921.36	883.14	-855,50	-508,48
20	2455464,29	-7,90	-74,53	155,8	-7,90	332	74	-112	4616.39	985.30	3056,90	743,45
21	2455717,07	-7,84	-74,46	154,2	-7,84	356	48	-81	2104.13	1863.18	-2081,70	-1715,56
22	2455798,24	-7,68	-74,66	144,4	-7,68	336	58	-114	739.93	356.30	-1081,82	-396,14
23	2456141,90	-8,58	-74,36	150,5	-8,58	16	67	-101	4781.96	2085.42	-1335,14	-685,17
24	2457158,56	-7,81	-74,42	160,7	-7,81	164	50	-106	2426.41	1851.44	1086,05	855,75
25	2457418,82	-8,25	-74,29	160,7	-8,25	172	90	75	1562.82	112.90	116,61	-23,85
26	2457448,87	-7,85	-74,38	155,6	-7,85	337	64	-119	1146.35	528.46	250,48	-146,38

No.	Date (days in JC)	Lat °	Lon °	Depth (km)	MI	NP2			MSBE		AEOT	
						S	D	R	$\sigma_N$ (Pa)	$\sigma_S$ (Pa)	$\sigma_N$ (Pa)	$\sigma_S$ (Pa)
27	2457704,12	-8,44	-74,53	148,4	-8,44	43	83	-42	4635.24	-223.14	5704,59	-200,58
28	2457877,60	-8,56	-74,42	156,1	-8,56	331	85	-69	1406.04	187.96	884,59	5,88